



**HAL**  
open science

# Variational estimation of effective channel and ungauged anabranching river discharge from multi-satellite water heights of different spatial sparsity

Pierre-André Garambois, Kévin Larnier, Jerome Monnier, Pascal Finaud-Guyot, Jonas Verley, Amanda Samine Montazem, Stéphane Calmant

## ► To cite this version:

Pierre-André Garambois, Kévin Larnier, Jerome Monnier, Pascal Finaud-Guyot, Jonas Verley, et al.. Variational estimation of effective channel and ungauged anabranching river discharge from multi-satellite water heights of different spatial sparsity. *Journal of Hydrology*, 2020, 581, pp.124409. 10.1016/j.jhydrol.2019.124409 . hal-03012617

**HAL Id: hal-03012617**

**<https://hal.science/hal-03012617>**

Submitted on 21 Dec 2021

**HAL** is a multi-disciplinary open access archive for the deposit and dissemination of scientific research documents, whether they are published or not. The documents may come from teaching and research institutions in France or abroad, or from public or private research centers.

L'archive ouverte pluridisciplinaire **HAL**, est destinée au dépôt et à la diffusion de documents scientifiques de niveau recherche, publiés ou non, émanant des établissements d'enseignement et de recherche français ou étrangers, des laboratoires publics ou privés.



Distributed under a Creative Commons Attribution - NonCommercial 4.0 International License

# Variational inference of effective channel and ungauged anabranching river discharge from multi-satellite water heights of different spatial sparsity

P.-A. Garambois(1)(2)(3)\*, K. Larnier(5)(2)(4)(6), J. Monnier (5)(6), P. Finaud-Guyot(7), J. Verley(5)(6), A.-S. Montazem(8)(9), S. Calmant (8)(9)

(1) *Now at: Irstea, Aix Marseille Univ, RECOVER, Aix-en-Provence, France*

(2) *ICUBE, CNRS, Univ Strasbourg, France.*

(3) *INSA Strasbourg, Strasbourg, France*

(4) *CS corporation, Business Unit Espace, Toulouse, France*

(5) *Institut de Mathématiques de Toulouse (IMT), France*

(6) *INSA Toulouse, France*

(7) *Now at: HSM, Univ Montpellier, CNRS, IRD, Montpellier, France*

(8) *LEGOS, UMR 5566, CNES, CNRS, IRD, UPS,*

(9) *Université de Toulouse III Paul Sabatier, OMP, Toulouse, France*

---

## Abstract

Multi-satellite sensing of continental water surfaces (WS) represents an unprecedented and increasing potential for studying ungauged hydrological and hydraulic processes from their signatures, especially on complex flow zones such as anabranching rivers. However the estimation of discharge from WS observations only is a very challenging, ill-posed, inverse problem due to unknown bathymetry and friction in ungauged rivers, measurements nature, quality and spatio-temporal resolutions regarding the flow (model) scales. This paper proposes an effective 1D hydraulic modeling approach of sufficient complexity to describe anabranching river flows from sparse multisatellite observations using the HiVDI inverse method presented in [1] with an augmented control vector including a spatially distributed friction law  $K(x, h)$  depending on the flow depth  $h$ . It is shown on 71km of the Xingu River (anabranching, Amazon basin) with altimetric water height timeseries that a fairly accurate upstream discharge hydrograph and effective patterns of channel bathymetry and friction can be inferred simultaneously. The coherence between the sparse observation grid and the fine hydraulic model grid is ensured in the optimization process by imposing a piecewise linear bathymetry profile  $b(x)$ , which is consistent with the *hydraulic visibility* of WS signatures ([2, 3]). The discharge hydrograph  $Q(t)$  at observation times and effective bathymetry-friction ( $b(x)$ ,  $K(x, h)$ ) patterns are retrieved from 8 years of satellite altimetry (ENVISAT) at 6 virtual stations (VS) along flow. Next, the potential of the forthcoming SWOT data, dense in space, is highlighted by inferring a discharge hydrograph and dense patterns of effective river bathymetry and friction; a physically consistent scaling of friction by reaches enables to consider more dense bathymetry controls. Finally a numerical analysis shows: (i) the importance of an unbiased prior information in the inference of a triplet  $(Q, b(x), K(x, h))$  from WS observations; (ii) the clear signatures of river bottom slope break in low flows and width variations in high flows, through the analysis of the friction slope term, which is consistent with the findings of [3] from WS curvature analysis.

15 *Keywords:* Anabranching River, Ungauged River, 1D Hydraulic Model, Variational Assimilation, Satellite  
16 Altimetry, SWOT, Hydraulic Visibility

---

17 Corresponding author: pierre-andre.garambois@irstea.fr

## 18 1. Introduction

19 Fresh water is a crucial earth’s resource and its journey from the clouds to the oceans passes through the hy-  
20 drographic network. In order to characterize hydrological fluxes, an essential physical variable is river discharge (cf.  
21 Global Climate Observing system [4]) representing an integration of upstream hydrological processes. In comple-  
22 ment of in situ sensors networks which are declining in some regions (e.g. [5]), increasingly accurate measurements  
23 of hydrological and hydraulic variables, and especially river surface variabilities are now enabled by myriads of  
24 satellites for earth observation and new generations of sensors (e.g. [6, 7, 8, 9]).

25 The forthcoming Surface Water and Ocean Topography (SWOT) wide swath altimetric mission (CNES-NASA,  
26 planned to be launched in 2021) will provide a quasi global river surfaces mapping with an unprecedented spatial and  
27 temporal resolution on Water Surface (WS) height, width and slope - decimetric accuracy on WS height averaged  
28 over 1 km<sup>2</sup>, 1 to 4 revisits every 21 days cycle [10, 11, 12, 13, 14]. In addition to decades of nadir altimetry (e.g.  
29 [15, 16, 17, 18]) and imagery (e.g. [19]) on inland waters, SWOT will enable an unprecedented *hydraulic visibility*,  
30 as defined from hydraulic analysis in [2, 20, 3], of hydrological responses and hydraulic variabilities within river  
31 networks. Multi-satellite observations of water surfaces from the local to the hydrographic network scale indeed  
32 represent an unprecedented observability of hydrological responses through hydraulic processes signatures, especially  
33 on complex flow zones such as floodplains or anabranching rivers (see river morphology classification in [21]). This  
34 increased *hydraulic visibility* represents a great potential to learn hydrodynamic behaviors and infer hydrological  
35 fluxes.

36 The estimation of river discharge from water surface observations (elevations, top width) remains an open and  
37 difficult question, especially in case of unknown or poorly known river bathymetry, friction or lateral fluxes. Several  
38 open-channel inverse problems are studied in a relatively recent litterature in a satellite data context with more  
39 or less complex flow models and inverse methods (cf. [13] for a review). Few studies started to highlight the  
40 benefits of assimilating synthetic SWOT WS observations in simplified hydraulic models with sequential methods,  
41 for inferring inflow discharge assuming known river friction and bathymetry [22, 23] or inferring bathymetry assuming  
42 known friction [24, 25]. Next, low-complexity methods have been proposed for estimating river discharge in case  
43 of unknown bathymetry and friction based on the kinematic wave assumption [26, 27] or hydraulic geometries  
44 [28] or empirical flow models ([29], see also [30]). They are tested on 19 rivers with synthetic “SWOT-like” daily  
45 observations in [29] and their robustness and accuracy is found to fluctuate, the importance of good prior guesses

46 is highlighted.

47 The combined use of dynamic flow models and optimization methods enables to benefit from WS observations  
48 for solving hydraulic inverse problems as shown for flood hydrograph inference in [31] from WS width time series  
49 used to optimize a 1D hydraulic model or in [32, 33, 34] by variational assimilation of flow depth time series in a  
50 2D hydraulic model. The variational data assimilation (VDA) approach (see e.g. [35] and references therein) is well  
51 suited to solve the present inverse problem (see [36, 37, 1] and references therein).

52 It consists in fitting the hydraulic model response to the observed WS elevations by optimizing the “input  
53 parameters” in a variational framework. However, altimetry measurements of WS are relatively sparse in time  
54 compared to local flow dynamics. This important aspect of the inverse problem is investigated in [36] with the  
55 introduction of *the identifiability maps*. The latter consist to represent in space-time the available information:  
56 WS observables, hydraulic waves and an estimation of the misfit with the local equilibrium. These “maps” enable  
57 to estimate if the sought upstream discharge information has been observed or not within the downstream river  
58 surface deformations; also they help to estimate inferable hydrograph frequencies [36] or inferable hydrograph time  
59 windows [1].

60 The inference of the hydraulic triplet (inflow discharge  $Q(t)$ , effective bathymetry  $b(x)$  and friction coefficient  $K$ )  
61 from SWOT like WS observations is investigated in recent studies using 1D hydraulic and variational assimilation  
62 methods (e.g. [36, 38, 37, 1]). However the inference of the triplet from WS observations remains a very challenging  
63 inverse problem because of the correlated influence of temporal (discharge) and spatial (bathymetry-friction) controls  
64 on the simulated flow lines. This is especially true because of the bathymetry-friction “equifinality issue”, see the  
65 discussions in [27, 1]. Those recently developed VDA methods enable to infer accurately the inflow discharge from  
66 water surface observables, considering unknown/uncertain channel bathymetry-friction, but from accurate prior  
67 information and synthetic WS observations. Note that a strong prior such as a known stage-discharge relationship  
68 (rating curve) downstream of a river domain as it is done in [37] can control part of the simulated flow lines (fluvial  
69 regime); as a consequence the VDA process may converge to the discharge hydrograph corresponding to the imposed  
70 (almost exact) rating curve. In the present study the downstream boundary condition (BC) is an unknown of the  
71 inverse problem.

72 A crucial point is the sensitivity of the triplet inference to the prior value from which the inference is started and it  
73 is studied in a SWOT observability context in [27, 39, 1, 40]. The sensitivity of the estimated discharge (in the triplet)  
74 to the prior is highlighted by recent estimates performed from AirSWOT airborne measurements on the Willamette  
75 River [40]. The temporal signal is well retrieved at observation times but using a biased prior hydrograph results in  
76 a biased hydrograph inference - see detailed investigations in [1]. In view to infer worldwide river discharges from  
77 the future SWOT observations, especially for ungauged cases, a hierarchical modeling strategy HiVDI (Hierarchical  
78 Variational Discharge Inversion) is proposed in [1]. The HiVDI approach includes low complexity flow relations  
79 (under the assumption of Low Froude and locally steady-state flows) which improves the robustness of the inferences

80 in particular if an (unbiased) average value of  $Q$  is provided. (It may be provided by a database or a regional  
81 hydrological model). Note that if introducing an a-priori information such as a single depth measurement, it enables  
82 to reconstruct an effective low-flow bathymetry see [41, 27, 1].

83 All the studies mentioned above mostly address single channel natural rivers ( $\sim 100\text{km}$  in length) without lateral  
84 inflows and using synthetic datasets (except in [40] with AirSWOT data). Moreover very few studies address the  
85 modeling of effective 1D channels from real satellite data (e.g. [2, 42]).

86 The present paper investigates the effective hydraulic modeling of anabranching river flows from real multi-  
87 sensor satellite observations of WS, the challenging inference of the hydraulic triplet  $(Q(t), b(x), K(x, h))$  and its  
88 sensitivity to observation density in space. Anabranching rivers are characterized by complex hydraulic geometries  
89 relationships across flow regimes as shown in [43] through an analysis of a metric resolution 2D shallow water  
90 model of an anabranching portion of the Platte River, US. The key point here is to build up a sufficiently complex  
91 model to describe anabranching river flows and in coherence with the spatio-temporal scales of satellite altimetry  
92 measurements.

93 Based on the inverse method presented in [1, 36], an effective hydraulic modeling strategy is adapted for tackling  
94 anabranching river flows using: (i) effective 1D cross sections based on real multi-satellite data from low to high  
95 flows (ii) a spatially distributed friction law depending on modeled water depth  $h$ . The inference of distributed  
96 hydraulic parameters patterns is investigated on a  $71\text{km}$  long reach of the Xingu River (Amazone basin) from real  
97 altimetric observations gained on a single ENVISAT track or from synthetic SWOT observations, low *identifiability*  
98 *index* (as introduced in [36] and detailed in section 4). The influence of the spatial density of WS observations on  
99 the identifiability of spatial controls patterns (in the unknown triplet) is studied. A piecewise linear bathymetry  
100 representation is introduced along with a friction power law with piecewise constant parameters to put in coherence  
101 the observations and the flow model grids. Their constraining effect on the inversions is studied with spatially  
102 (and temporally) sparse satellite observations. Furthermore, numerical investigations are performed to test the  
103 sensitivity of hydraulic inferences to prior hydraulic values and also assess the correlated influence of bathymetry  
104 and friction on the modeled flow lines (equifinality) across flow regimes.

105 This study is organized as follows. Section 2 presents the 1D Saint-Venant flow model and the effective modeling  
106 approach for anabranching rivers including: (i) a spatially distributed friction law depending on the modeled flow  
107 depth, (ii) the construction of an effective channel geometry from multi-satellite observations, (iii) an inverse method  
108 based on variational data assimilation. Section 3 focuses on the calibration of the effective model on 8 years of  
109 WS observations gained from ENVISAT altimeter on a single track along this anabranching river. Using this  
110 model as a reference, section 4 proposes detailed investigations of the hydraulic inferences from real ENVISAT  
111 or synthetic SWOT observations considering this anabranching river as ungauged. The discussion in section 5  
112 presents a numerical sensitivity analysis to the hydraulic prior and some investigations on the bathymetry friction  
113 equifinality.

114 **2. Modeling approach:**

115 This section proposes an original 1D effective modeling approach of adequate complexity for modeling anabranch-  
 116 ing river flows across (fluvial) regimes and in coherence with satellite observations. The approach is built on an  
 117 effective channel cross-section derived from multi-satellite measurements and a spatially distributed friction law  
 118 depending on the flow depth.

119 *2.1. The flow model*

120 River flows are classically modeled using the 1D Saint-Venant shallow water equations involving an integration  
 121 of the flow variables over the cross section (see e.g. [44, 45] for detailed assumptions). In  $(A, Q)$  variables,  $A$  the  
 122 wetted-cross section  $[\text{m}^2]$ ,  $Q$  the discharge  $[\text{m}^3.\text{s}^{-1}]$ , the equations read as follows [44]:

$$123 \quad \begin{cases} \partial_t(A) + \partial_x(Q) & = 0 \\ \partial_t Q + \partial_x \left( \frac{Q^2}{A} \right) & = -gA \partial_x Z - gAS_f \end{cases} \quad (1)$$

124 where  $g$  is the gravity magnitude  $[\text{m}.\text{s}^{-2}]$ ,  $Z$  is the WS elevation  $[\text{m}]$ ,  $Z = (b+h)$  with  $b$  is the river bottom elevation  
 125  $[\text{m}]$  and  $h$  is the water depth  $[\text{m}]$ . The friction slope  $S_f$  is parameterized with the classical Manning-Strickler law  
 126 such that  $S_f = |Q|Q/K^2 A^2 R_h^{4/3}$  with  $K$  the Strickler friction coefficient  $[\text{m}^{1/3}.\text{s}^{-1}]$ ,  $R_h = A/P_h$  the hydraulic radius  
 127  $[\text{m}]$ ,  $P_h$  the wetted perimeter. The discharge  $Q$  is related to the average cross-sectional velocity  $u$   $[\text{m}.\text{s}^{-1}]$  such as  
 128  $Q = uA$ . A spatially distributed Strickler friction coefficient is defined as a power law in the water depth  $h$ :

$$129 \quad K(x, h(x, t)) = \alpha(x)h(x, t)^{\beta(x)} \quad (2)$$

130 where  $\alpha$  and  $\beta$  are two constants. Similar approaches based on hydraulic geometry or power law resistance equations  
 131 are developed in the litterature for predicting mean flow velocity for example on a wide range of in situ river flow  
 132 measurements in [46] or else for gravel bed streams in [47]. The friction depends on the flow depth through the  
 133 proposed power law relation (Eq. 2) enabling a variation of the friction effect in function of the flow regime for  
 134 complex flow zones for instance; this spatially distributed friction law is richer than a constant uniform value as it  
 135 is often set in the literature from a-priori tables of frictions in function of river types for instance (e.g. [48]).

136 Note that satellite altimetry mostly observes the downstream parts of river networks (top width  $W > 100\text{m}$  for  
 137 SWOT), mainly in subcritical and mostly low Froude flows at the observation scales (cf. [49, 1, 3]). The discharge  
 138  $Q_{in}(t)$  is classically imposed upstream of the river channel with a discharge hydrograph. At downstream a normal  
 139 depth is imposed using the Manning-Strickler equation depending on the unknowns  $(A, Q; K)_{out}$  (it is classically  
 140 integrated in the Preissmann scheme equations). The initial condition is set as the steady state backwater curve  
 141 profile  $Z_0(x) = Z(Q_{in}(t_0))$ ; also depending on the unknowns. Note that these boundary and initial conditions  
 142 are updated during the iterative inverse method presented in what follows. This 1D Saint-Venant model (Eq. 1)

143 is discretized using the classical implicit Preissmann scheme (see e.g. 50) on a regular grid of spacing  $\Delta x$ . It is  
144 implemented into the computational software DassFlow (DassFlow [51]).

## 145 2.2. Effective anabranching river model from multisatellite data

146 A  $L = 71\text{km}$  long portion of the Rio Xingu containing anabranching reaches is considered (Fig. 1, cf. [2]). WS  
147 observations are available at 6 virtual stations along a single ENVISAT track (#263) representing 77 samples of  
148 WS profiles between mid 2002 and mid 2010 (cf. [17]); that is  $\{Z_{s,p}^{obs}\}_{S,P}^{env}$  with  $S = 6$  corresponding to the locations  
149 of the virtual stations simultaneously observed at  $P = 77$  times (see Tab. 1).

150 An effective hydraulic modeling strategy of this anabranching river is proposed based on:

- 151 • Cross-sectional water surface widths  $\{W\}_{S,2}^{jers}$  obtained from JERS mosaics (Courtesy of GRFM, NASDA/MITI)  
152 in low and high flows. The effective water surface width is the sum of the width of all individual river channels  
153 for anabranching reaches. Note that the cross section geometry of this (ungauged) anabranching river might  
154 be changing over a hydrological year, from “disconnected channels” in low-flows to a “mono-channel” with  
155 forested floodplains during the flood season. The available satellite images resulted in an estimation of a  
156 larger effective top width in high-flow.
- 157 • An a priori river bottom  $\{b\}_{TVS}$  obtained from altimetric rating curves from [52]. The authors determined  
158 effective bottom elevations by adjusting the scalar parameters  $\gamma$  and  $\delta$  of a classical stage discharge relationship  
159  $Q = \gamma(Z - b)^\delta I^{1/2}$ , with  $I$  the water surface slope gained from altimetry at large scale. They used WS  
160 elevations gained by satellite altimetry and discharges simulated with the large scale hydrological model MGB  
161 ([53, 54, 55]) on the temporal window of interest - called true discharge in what follows.

162 Effective cross-sections geometries are defined at the 6 virtual stations with the bathymetry  $b$  given by altimetric  
163 rating curves and from effective widths such that low flow width (resp. high flow) is reached for the first (resp.  
164 ninth) decile of observed WS elevations for each cross section. The final model geometry is obtained by linear  
165 interpolation between these 6 effective cross sections on the model grid with  $\Delta x = 50m$ . It is shown in Fig. 1 along  
166 with ENVISAT and SWOT spatial samplings. The friction law (Eq. 2) introduced above and depending on the flow  
167 depth  $h$  is distributed using patches with constant values for each reach between two successive virtual stations.

168

## 169 2.3. The computational inverse method

170 This paper investigates the estimation of the hydraulic triplet  $(Q(t), b(x), K(x, h))$  from observations of WS  
171 variabilities only on an anabranching river. The employed inverse method is those presented in [1] (see also [36])  
172 with an augmented composite control vector  $c$ ; it is detailed in Appendix 7.  $c$  contains a spatially distributed  
173 friction coefficient enabling to model complex flow zones (while it is an uniform friction law  $K(h)$  in [1]). This  
174 definition of  $K(x, h)$  enables to consider more heterogeneous bathymetry controls.

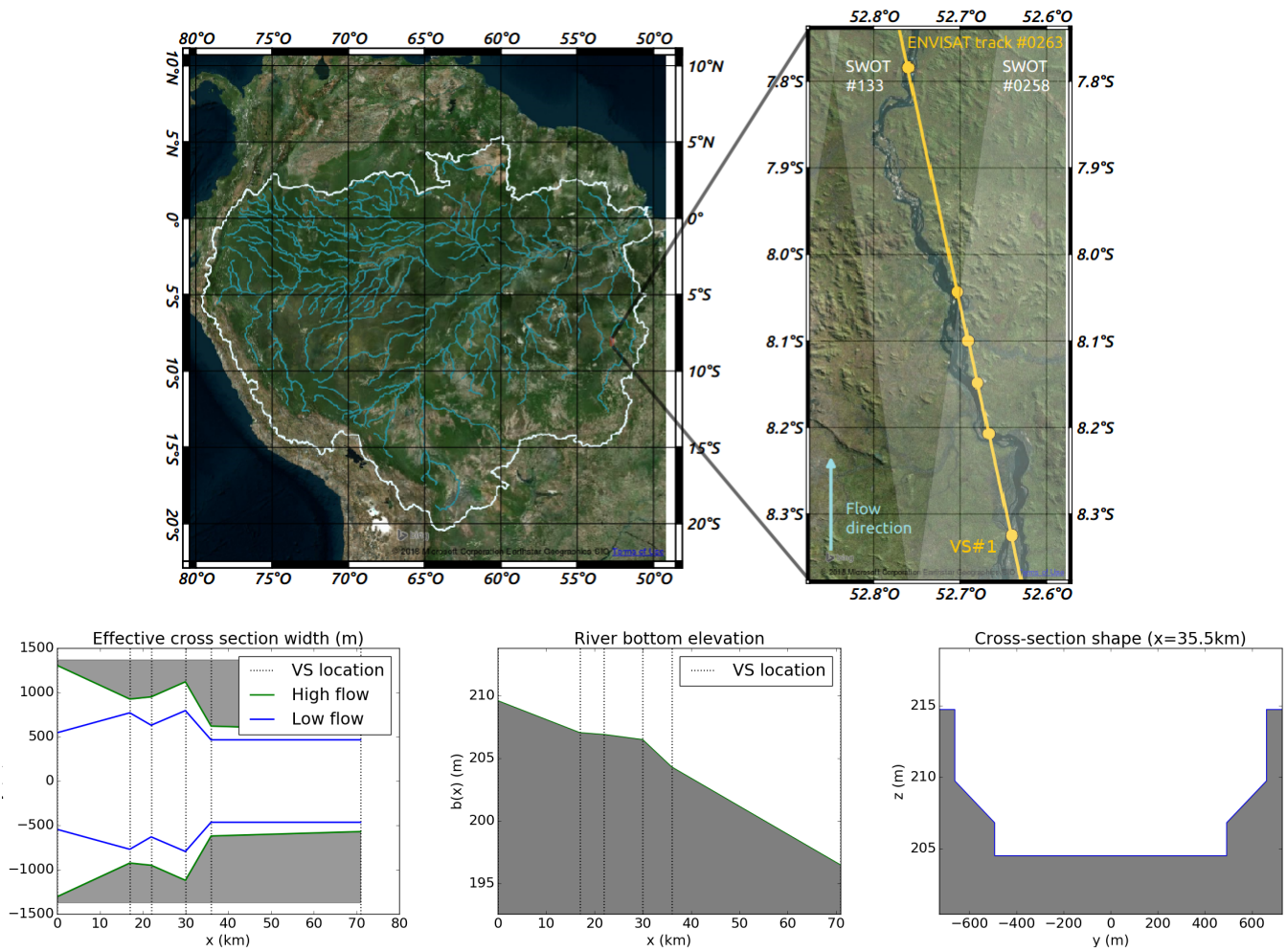


Figure 1: Study zone (top) with ENVISAT track #263 and virtual stations (orange dots); simulated SWOT tracks #133 and #258 on the 1<sup>st</sup> and 6<sup>th</sup> day every 21 days repeat cycle (transparent white). Effective river bathymetry derived from altimetric rating curves ([52]) and water surface width from satellite images.

175 The principle is to estimate (discrete) flow controls minimizing the discrepancy between  $Z_{obs}$  the observed flow  
 176 line and  $Z$  the modeled one; the latter depending on the unknown parameters vector  $c$  through the hydrodynamic  
 177 model (Eq. 1). This discrepancy is quantified through the cost function term:

$$j_{obs}(c) = \frac{1}{2} \|Z_{obs} - Z(c)\|_2^2 \quad (3)$$

178  
 179 see Appendix 7 for details. The control vector  $c$  contains the unknown “input parameters” of the 1D Saint-Venant  
 180 shallow water flow model (Eq. 1) considering effective cross sections (see Fig. 1). In the present study,  $c$  reads as:

$$c = (Q_{in,0}, \dots, Q_{in,P}; b_1, \dots, b_R; \alpha_1, \dots, \alpha_N, \beta_1, \dots, \beta_N)^T \quad (4)$$

181  
 182 where temporally and spatially distributed controls are the upstream discharge  $Q_{in,p}$ , the river bed elevation  $b_r$  and  
 183 the distributed friction parameters  $\alpha_n$  and  $\beta_n$ .

184 The subscript  $p$  denotes the observation time  $p \in [0..P]$  and  $r$  denotes the reach number,  $r \in [1..R]$ .

185  $\alpha_n$  and  $\beta_n$  are the parameters of the friction law depending on the model state  $h$  (Eq. 2) for each patch  $n \in [1..N]$   
 186 with  $N \leq R$ .

187 The inversion consists to solve the following minimization problem:  $c^* = \text{argmin } j(c)$  (Eq. 9).

188 This minimization, optimization problem is solved using a first order gradient-based algorithm, more precisely  
 189 the classical L-BFGS quasi-Newton algorithm. The main steps of the method are illustrated in Fig. 2.

### 191 3. Model Calibration

192 This section presents the calibration of the effective hydraulic model based on the reference effective geometry  
 193 defined above (cf. section 2.2). The observed water elevation time series  $\{Z_{s,p}^{obs}\}_{S,P}^{env}$  at  $S = 5$  ENVISAT virtual  
 194 stations are used to calibrate the friction law of the 1D Saint-Venant flow model (Eq. 1). Since friction has a local  
 195 and upstream influence on a flow line (low Froude fluvial flows, Fig. 10) the remaining ENVISAT time series at  
 196 VS#6 downstream of the river domain will be used for inferring the full control vector  $c$  in next section - recall that  
 197 a normal depth is used as downstream BC (cf. section 2.1).

198 A “reduced” control vector  $c_{cal} = (\alpha_1, \dots, \alpha_N, \beta_1, \dots, \beta_N)$  consisting in spatially distributed friction parameters  
 199 only is considered here. In order to avoid a spatial “overparameterization” regarding the 5 water height timeseries  
 200 available at VS, the choice is made to spatialize friction on  $N = 5$  patches, on each reach downstream an altimetric  
 201 VS. The inverse method presented in [1] and described in appendix (section 7) is used here with no regularization  
 202 nor variable change for this “simple” calibration problem.

203 An optimal friction distribution  $c_{cal}^*$  is found with the inverse method and the calibrated values of  $\alpha_{n=1..5}$  and  
 204  $\beta_{n=1..5}$  are summed up in Tab. 1. The resulting water height time series are compared to altimetric observations

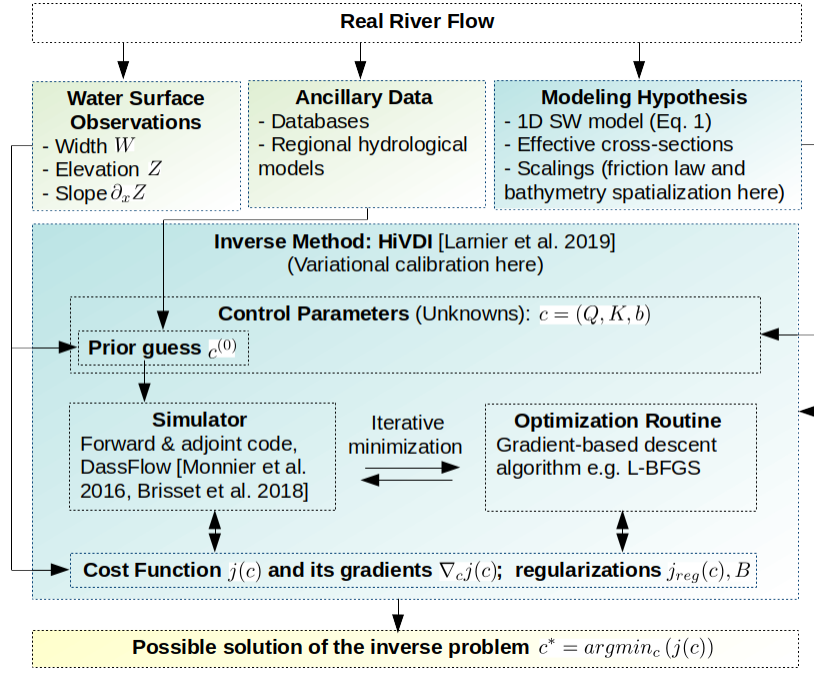


Figure 2: Flowchart of the method using the HiVDI inverse method (Larnier et al. [1]) for variational calibration, adapted from Monnier et al. [56], Monnier [57].

205 for each virtual station (cf. Fig. 3). The spatially distributed friction law (Eq. 2) enables a fairly good reproduction  
 206 of the observed water level variations on this anabranching river, across a wide range of flows, even with an effective  
 207 1D model built on multi-satellite data (Fig. 3).

208 A constant friction in time would lead to systematical errors for a large range of flows as shown by the grey  
 209 curves on Fig. 3. The calibrated friction exponents  $\beta_n$  range between 0.482 and 1.133 except for the second reach  
 210 (SV2-3) where a small  $\beta_n$  is found, that is a barely constant friction across flow regimes for this short reach (cf. Fig.  
 211 3). The spatial pattern of  $\alpha_n$  values calibrated here corresponds to significant friction effects, varying across flow  
 212 regimes, and necessary to effectively represent anabranching reaches using a 1D effective cross section. Indeed the  
 213 latest leads to an underestimation of the hydraulic radius  $R_h = A/P_h$  hence of the friction slope  $S_f = |Q|Q/K^2A^2R_h^{4/3}$   
 214 in the 1D Saint-Venant model (see section 2.1) for anabranching reaches.

215  
216

#### 217 4. Inferences of distributed spatio-temporal flow controls ( $Q(t), K(x, h), b(x)$ ) from WS observations

218 This section studies the challenging inference of the hydraulic triplet (discharge, bathymetry, friction) from  
 219 multi-satellite WS observations. The anabranching Xingu River morphology represents a supplementary difficulty  
 220 for inversions regarding the variability of local hydraulic behaviors across flow regimes as evidenced above by  
 221 the calibrated friction laws ( $\beta^{cal} \neq 0$ ). The impact of spatial controls density and bathymetry representation is

Virtual station name	VS#1	VS#2	VS#3	VS#4	VS#5	VS#6
Flow distance to mouth [km]	1146	1129	1124	1116	1110	1075
Flow distance from the upstream [km]	0	17	22	30	36	71
Drainage area [km <sup>2</sup> ] (MGB model)	193.255	193.255	194.148	194.148	195.882	197.862
$Z_0$ [m] (reference : EGM2008) (Paris et al. 2016)	209.6	207.1	206.9	206.5	204.3	196.5
$W_{low}(x)$ Total low flow width [m] (derived from JERS)	1090	1540	1260	1590	930	930
$W_{high}(x)$ Total high flow width [m] (derived from JERS)	2610	1850	1900	2240	1240	1140
Calibrated friction factor $\alpha^{cal}(x)$ (downstream reach)	12.785	19.574	9.869	4.252	7.425	-
Calibrated friction exponent $\beta^{cal}(x)$ (downstream reach)	0.482	0.071	0.624	1.133	0.718	-

Table 1: Summary of the effective hydraulic model parameters including calibrated friction parameters  $\alpha^{cal}(x)$  and  $\beta^{cal}(x)$  (recall  $K(x, h) = \alpha(x)h^{\beta(x)}$ ) using 8 years of WS elevation variations (ENVISAT data) given effective channel bathymetry and upstream discharge from the MGB hydrological model ([54]).

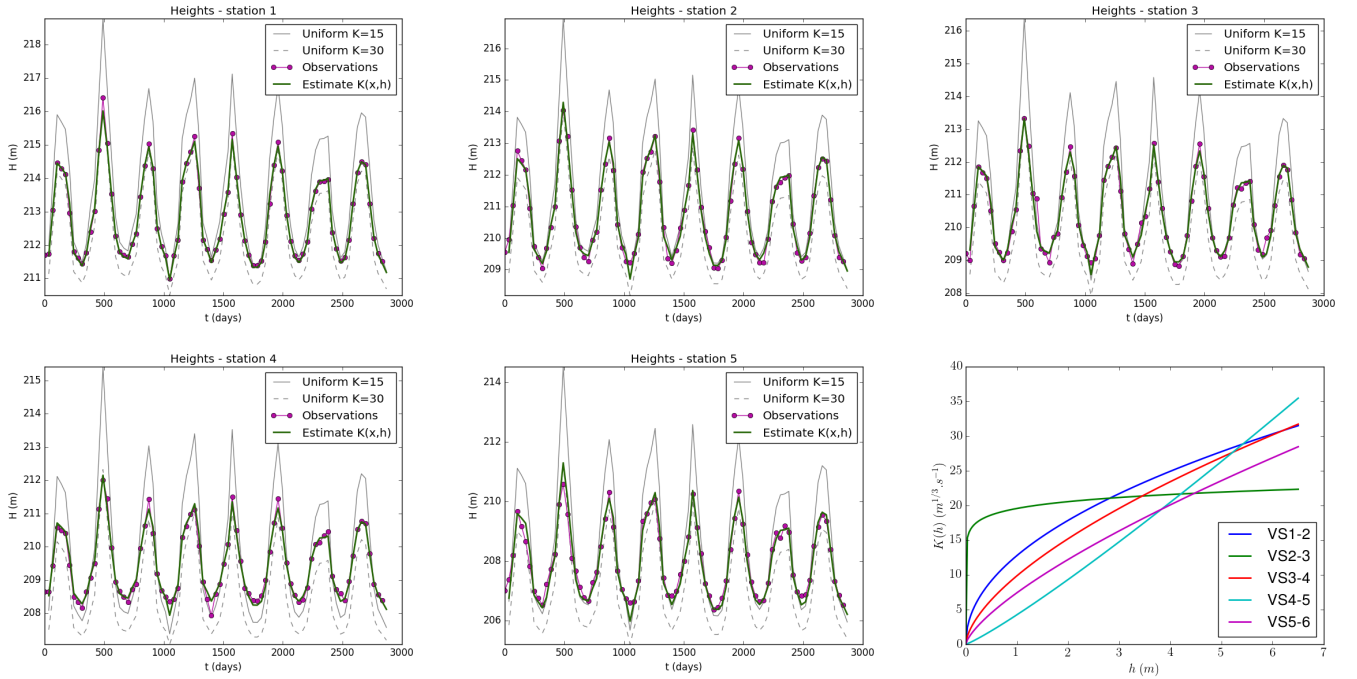


Figure 3: Calibration of variable friction  $K(x, h)$  with 8 years of ENVISAT measurements at 6 VS using the variational method with  $c = (\alpha_1, \dots, \alpha_5, \beta_1, \dots, \beta_5)$ ;  $j_{obs} = 0.07$ . (Bottom right) Effective friction law in function of water depth for each VS.

222 assessed in what follows regarding the spatial sparsity of observations. First is presented the numerical experiment  
 223 framework, then the inferences with relatively “sparse” ENVISAT measurements and finally those with SWOT  
 224 synthetic observations.

#### 225 4.1. Design of the numerical experiments

226 The effective hydraulic model described in section 2.2 and calibrated in section 3 is used as a reference (“target”)  
 227 in the following numerical experiments. The control vector (Eq. 4) containing discharge, bathymetry and friction  
 228 is sought with the inverse method described in section 2.3 (see also appendix, section 7). It is tested first with real  
 229 ENVISAT time series representing a relatively sparse spatial sampling of WS signatures with 6 VS on this 71km  
 230 long river, and next with synthetic SWOT observations sampling the flow line at  $\Delta x = 200m$  (RiverObs product,  
 231 see [58]).

232 The Xingu River is observed either by a single along-stream ENVISAT track at 6 observation points (virtual  
 233 stations) of flow lines every 35 days, or two SWOT tracks providing dense WS observations in space twice per  
 234 21 days repeat cycle (5 days delay, cf. section 2.2). Note that the temporal sparsity of observations (35 days  
 235 for ENVISAT or 5 days between the two SWOT passes every 21 days) only enables to identify low hydrograph  
 236 frequencies, at observation times (see [36] for a detailed analysis and the identifiability maps). Indeed the hydraulic  
 237 wave propagation time is around  $T_{wave} \sim 9h$  which is much smaller than the lowest satellite revisit time of 5 days.  
 238 This propagation time is calculated using the kinematic wave velocity for rectangular channels  $c_k = 5/3U$  and  
 239 maximal high flow velocity  $U = 2.17m/s$  from calibrated model outputs  $c_k = 2.2m/s$  (second hydrograph peak  
 240 at  $t = 490 days$ , see flow variables on Fig. 10). Let  $I_{ident} = T_{wave}/\Delta t_{obs}$  be the identifiability index defined  
 241 in [36] as the ratio between flood wave propagation time and observation time step. This leads to a very low  
 242 temporal identifiability index for this 71km river:  $I_{ident} = 7.5 \times 10^{-2}$  for SWOT and  $I_{ident} = 10^{-2}$  for ENVISAT.  
 243 Consequently, only low temporal dynamics and discharge at observation times are inferable as shown in [36]; SWOT  
 244 and ENVISAT observations are thus considered separately in the present study.

245 The starting point of the VDA process in the parameter space, the so-called prior  $c_{prior}$  (cf. section 7), consists  
 246 in a rough hydrological prior:  $Q^{(0)} = \bar{Q}_{MGB}$  the mean discharge estimated from the MGB hydrological model,  
 247 a spatially constant  $\alpha^{(0)}$  friction defined a priori from classical hydraulic ranges (e.g. [48]) and  $\beta^{(0)} = 1$ , the  
 248 bathymetry  $b^{(0)}$  is defined as a simple straight line over the whole domain for hydraulic analysis first. Note that  
 249 the sensitivity of the inference to the prior definition is investigated in section 5.

250 In a noised observation context, we denote by  $\delta$  the noise level such that  $\|Z_{obs} - Z_{true}\|^2 \leq \delta$  for all spatial  
 251 locations  $r$  with  $Z_r^{obs}$  the observed and  $Z_r^{true}$  the true WS elevation. A common technique to avoid overfitting noisy  
 252 data, in the context of Tykhonov’s regularization of ill-posed problems, is Morozov’s discrepancy principle, (see e.g.  
 253 [59] and references therein): the regularization parameter  $\gamma$  (see Eq. 7) is chosen *a-posteriori* such that  $j$  does not  
 254 decrease below the noise level. In the present numerical experiments, the convergence is stopped if  $j_{obs}(c) \leq 10^{-1}$   
 255 or if  $j_{obs}$  is not decreased anymore for higher discrepancies.

256 4.2. Inference from spatially sparse ENVISAT snapshots

257 In this section the assimilation is based on WS elevations  $\{Z_{s,p}^{env}\}_{S,P}$  at  $S = 6$  virtual stations observed simul-  
258 taneously by ENVISAT during 8 years every 35 days, i.e.  $P = 77$ . In this spatially sparse observation context, the  
259 impact of spatial controls density is investigated.

260 First, we consider a “full” control vector  $c$  (cf. Eq. 4) including  $P = 77$  inflow discharges, all 1D model  
261 bathymetry points  $R = 1420$  and  $N = 5$  friction patches between ENVISAT virtual stations (cf. section 2.2).  
262 The inferred inflow discharge, bathymetry and friction are presented in Fig. 4 (case Env.a). Despite the satisfying  
263 value of the hydraulic controls reached at iteration 35, the descent is still possible as shown by  $j_{obs}$  decreasing of  
264 about 20% at iteration 96. Although it enables to fit the observations according to the a priori convergence criteria  
265 defined in section 4.1, the solution found after the VDA process is not very accurate nor realistic as shown by peak  
266 flow underestimations and significant oscillations of the identified friction and bathymetry. The spatial sparsity of  
267 observations prevents to infer these relatively dense bathymetry controls; in this case the considered inverse problem  
268 is underconstrained.

269 In order to better constrain the inverse problem in case of sparse spatial observability, a bathymetry represen-  
270 tation is consistently introduced at the scale of the observation grid and applied to the finer flow modeling grid.  
271 Based on the physical analysis of the SW model (Eq. 1) behaviour and the WS signature of bathymetry/friction  
272 controls (see [20, 60, 3]), a linear bathymetry interpolation is used between the successive couples of bathymetry  
273 controls defined at observation points only. The resulting bathymetry  $\tilde{b}(x) \in \mathcal{C}^0(\mathbb{R}), \forall x \in [0, L]$  is piecewise linear  
274 and strongly constrains the bathymetry profile between the sought bathymetry points - instead of using only a weak  
275 constraint  $j_{reg}(c) = \frac{1}{2} \|b''(x)\|_2^2$  in the optimization process (cf. appendix 7) as done in the next section 4.3 with  
276 spatially dense SWOT observations. Using this bathymetry constraint with  $R = 6$  bathymetry controls defined at  
277 each ENVISAT virtual station results in 5 reaches and  $N = 5$  friction patches are consistently applied to each. This  
278 leads to a more robust and accurate inference as shown in Fig. 5 (case Env.b). The discharge inferred for 8 years  
279 is fairly correct (RMSE = 520 m<sup>3</sup>/s, Nash = 0.95) and relatively realistic bathymetry/friction patterns are found,  
280 with some compensations between spatial controls locally in space, which is further analyzed in what follows.

281 The impact, on the inferred parameters, of searching a spatially uniform friction law is tested with the piecewise  
282 linear bathymetry representation used above. The resulting discharge inference is fairly correct (RMSE = 608 m<sup>3</sup>/s,  
283 Nash = 0.93) and interestingly the bathymetry spatial pattern is well retrieved but shifted above the reference one  
284 (cf. Fig. 6) (case Env.c). The inferred friction coefficients are  $\alpha = 22.621$ ,  $\beta = 0.217$ , which represents a lower  
285 friction effect on most flow regimes regarding the calibrated ones (cf. Tab. 1). These inferred effective friction  
286 law and bathymetry patterns, leading to somehow effective stage-discharge relationships locally given the inferred  
287 hydrograph and its propagation, enable to approximate the observed WS variations ( $j_{obs} = 1.269$ ) but with a less  
288 accurate fit than with spatially distributed friction ( $j_{obs} = 0.118$ ). Note that in this case of lower model complexity  
289 an underestimation of the low flow discharges occurs.

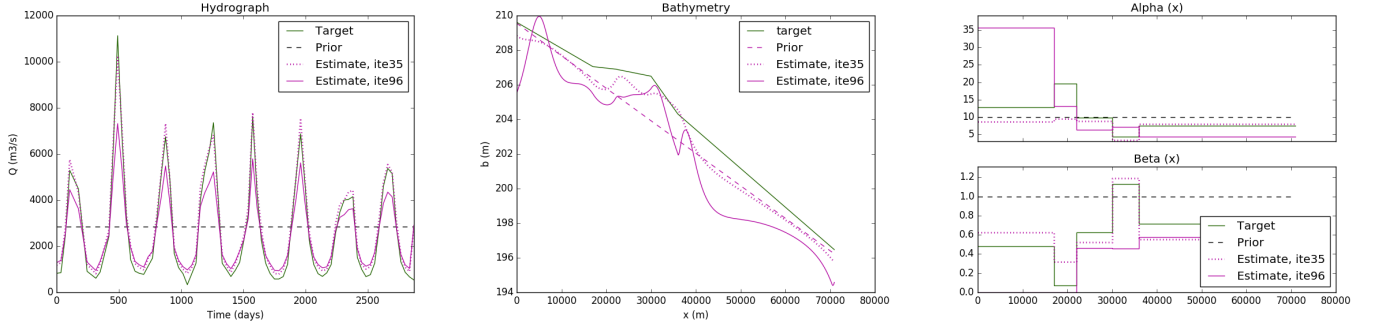


Figure 4: Identification of  $(Q(t), K(x, h), b(x))$  with ENVISAT observations and overparameterized  $c = (Q_{in,0}, \dots, Q_{in,P}; b_1, \dots, b_R; \alpha_1, \dots, \alpha_N, \beta_1, \dots, \beta_N)^T$  with  $P = 77$ ,  $R = 1420$ ,  $N = 5$ , bathymetry regularization weight  $\gamma = 10^{-3}$ ;  $j_{obs} = 0.098$  at iteration 35 (top) and  $j_{obs} = 0.077$  at iteration 96 (bottom) (Env.a)

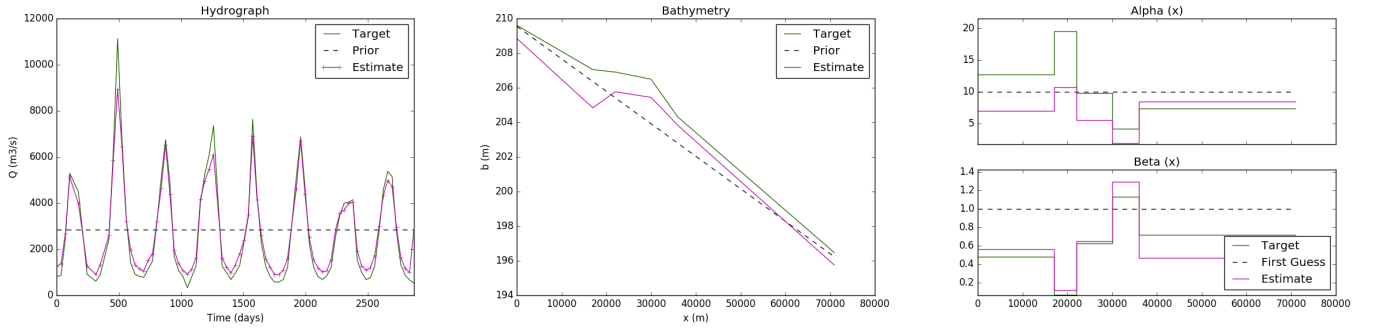


Figure 5: Identification of  $(Q(t), K(x, h), b(x))$  with ENVISAT observations and effective  $c = (Q_{in,0}, \dots, Q_{in,P}; b_1, \dots, b_R; \alpha_1, \dots, \alpha_N, \beta_1, \dots, \beta_N)^T$  with  $P = 77$ ,  $R = 6$ ,  $N = 5$  with a piecewise linear bathymetry  $b(x)$  reconstruction,  $\gamma = 0$ ;  $j_{obs} = 0.118$  at iteration 51. (Env.b)

290 Recall that the observations consist in real measurements of WS elevations gained by nadir altimetry on  
 291 anabranching reaches of the Xingu River. The complexity of the forward-inverse modeling approach, in coher-  
 292 ence with the spatial sparsity of the observation grid, enables to approximate satisfactorily the one of the observed  
 293 anabranching flow. The additional constraint provided by spatially dense flow lines observations is investigated in  
 294 the next section with SWOT synthetic data.

295

296

297

298

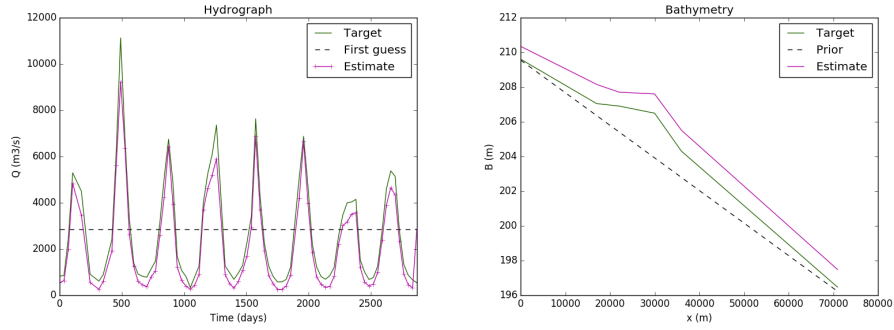


Figure 6: Inference of  $Q(t)$ ,  $b(x)$  and spatially uniform  $K(h) = \alpha h^\beta$  with ENVISAT WS observations and effective  $c = (Q_{in,0}, \dots, Q_{in,P}; b_1, \dots, b_R; \alpha, \beta)^T$ ,  $P = 77$ ,  $R = 6$ , no bathy  $\gamma = 0$ ;  $j_{obs} = 1.269$  at iteration 54. The identified friction coefficients are  $\alpha = 22.621$ ,  $\beta = 0.217$ . (Env.c)

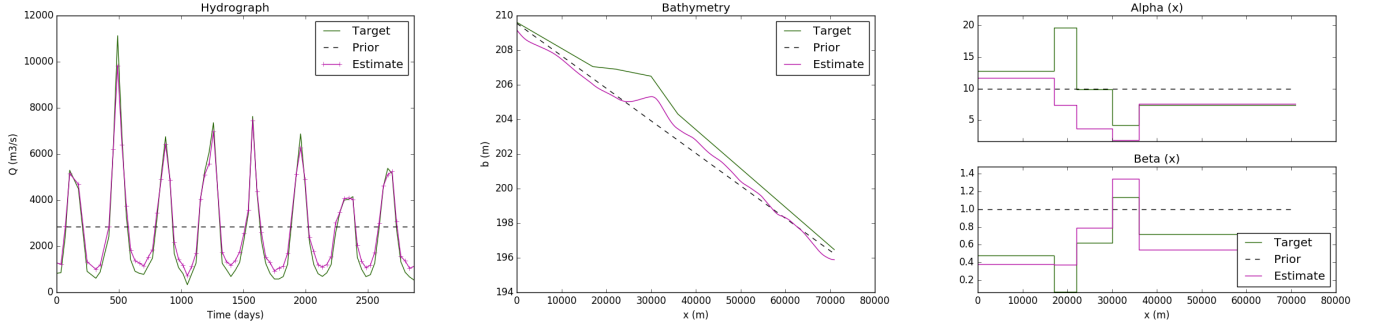


Figure 7: Identification of  $(Q(t), K(x, h(x, t)), b(x))$  with SWOT-sge observations and effective  $c = (Q_{in,0}, \dots, Q_{in,P}; b_1, \dots, b_R; \alpha_1, \dots, \alpha_N, \beta_1, \dots, \beta_N)^T$  with  $P = 276$ ,  $R = 1420$ ,  $N = 1419$ ,  $\gamma = 10^{-3}$ ;  $j_{obs} = 0.099$  at iteration 41. (SWOT.a)

### 299 4.3. Inference from spatially dense SWOT snapshots

300 In this section the full hydraulic control  $c$  (cf. Eq. 4) is inferred by assimilating SWOT-like observations. Those  
 301 noisy data are computed using the SWOT hydrology simulator applied to flow lines from the effective hydraulic  
 302 model calibrated above (cf. section 3). The SWOT spatio-temporal pattern over the studied river is obtained  
 303 by overlapping the river centerline and the expected SWOT orbit and swaths (cf. Fig. 1). Finally the synthetic  
 304 SWOT-like observables consist in WS elevations  $\{Z_{obs}^{SWOT}\}_{r,p}$  with  $p \in [1..P]$  and  $P = 276$  generated on the fine  
 305 scale model grid i.e.  $r \in [1..1420]$ .

306 The inflow discharge, bathymetry and friction are inferred by assimilating SWOT WS observations  $\{Z_{obs}^{SWOT}\}_{r,p}$   
 307 on the same spatial grid as that of the numerical hydraulic model with  $c_{prior1}$ . The estimates are presented on  
 308 Fig. (7). The inferred discharge hydrograph is accurate (RMSE =  $391 \text{ m}^3/\text{s}$ , Nash = 0.97) and bathymetry/friction  
 309 patterns are relatively well retrieved. Using SWOT spatially distributed observations and piecewise constant friction  
 310 enable to constrain the inference of bathymetry controls at a fine spatial resolution (model grid). The inverse  
 311 method includes: (i) a regularization term  $j_{reg}$  in the cost function (Eq. 7); (ii) covariance matrices acting as  
 312 spatial or temporal smoothers/regularizations (cf. Eq. 12 in appendix). The inferred discharge and spatially  
 313 distributed controls are slightly more accurate than previously in a comparable inversion scenario with sparse  
 314 ENVISAT observations in space and piecewise linear bathymetry constrain (case Env.b, cf. Tab. 2 and Fig. 5).  
 315 Note that the friction is sought by reaches which enables to consider more dense bathymetry controls. Again,  
 316 the compensation between spatial controls appears locally in space but enables the best fit to the distributed  
 317 measurements of WS elevations given the inferred discharge ( $j_{obs} = 0.099$ ).

318

## 319 5. Discussion and numerical investigation of the bathymetry-friction equifinality

320 This section discusses the challenging inference of spatially and temporally distributed river flow controls from  
 321 water surface observations through numerical investigations. Indeed, the considered flow controls  $(Q(t), b(x),$

322  $K(x, h)$ ) have a correlated influence and can produce undiscernable signatures in the modeled flow lines therefore  
323 leading to an ill-posed inverse problem (cf. [27, 1] for investigations on this “*bathymetry-friction equifinality*” in a  
324 comparable data-inversion context). The hydrograph is responsible for flow variability in time, hence enabling to  
325 retrieve the temporal dynamics of the observed flow lines [36, 1].

326 Given altimetric measurements of WS variabilities and the first guess  $c_{prior1}$ , the regularized inverse method  
327 enables to infer a complex control vector composed of temporally and spatially distributed controls of the 1D  
328 SW model (Eq. 1). In the numerical experiments above, the discharge hydrograph  $Q(t)$  is accurately inferred at  
329 observation times but because of the ill-posedness of the inverse problem, compensations can occur between the  
330 sought parameters and especially between the spatial controls - the bathymetry  $b(x)$  and the distributed friction  
331 parameters  $\alpha(x)$  and  $\beta(x)$ . These inferred friction laws and bathymetry patterns - simultaneously inferred with the  
332 discharge hydrograph - correspond to “effective rivers” enabling to fit the observed variability of flow lines.

333 Note that the spatial density of SWOT data enables to constrain flow controls that are relatively dense in space,  
334 here on a complex anabranching flow case using the effective 1D river representation and a friction law pattern  
335 depending on water depth. Improving the physical segmentation, parameterization and sparse representation of  
336 river networks and flow signatures (e.g. [3]) seems of great importance to take advantage of the forthcoming SWOT  
337 observations along with other data.

338 Importantly, as already pointed out in the VDA inferences performed with the DassFlow model using SWOT like  
339 data in [36, 1] and AirSWOT data in [40], the accuracy of the inferred discharge depends on the quality of the prior.  
340 In other words spatially distributed WS observations enable to depict spatio-temporal signatures and eventually  
341 propagation dynamics but a *quantitative biais* remains regarding fluxes, from the river reach to the network scale.

342 In the following subsection the influence of the prior value on the quality of the inferences with spatially  
343 distributed controls is investigated first. Next, is proposed a numerical analysis of the sensitivity of the friction  
344 slope (source term)  $S_f$  in the Saint-Venant equations (Eq. 1) to the flow controls (triplet) that are embedded in it  
345 (Manning-Strickler parameterization).

### 346 5.1. Sensitivity to the prior guess

347 The sensitivity of the inference to the quality of the prior guess of the control vector  $c_{prior}$  is investigated here  
348 for the most challenging inverse problem with spatially and temporally distributed controls and sparse ENVISAT  
349 data. First the inflow prior is varied of  $\pm 30\%$  around the mean true discharge; the river bottom elevation and  
350 friction priors are set as previously in  $c_{prior1}$ . The inferred hydraulic controls are presented in Fig. 8 and various  
351 inference scores are summed up in Tab. 2. For each inflow prior, the temporal variations of the inflow hydrograph  
352 are very well retrieved as shown on Fig. 8 - runs Env.b2 and Env.b3. However a biased inflow prior results in a  
353 biased hydrograph estimate (with correct temporal variations at observation times) which is coherent with results  
354 of [1, 40]).

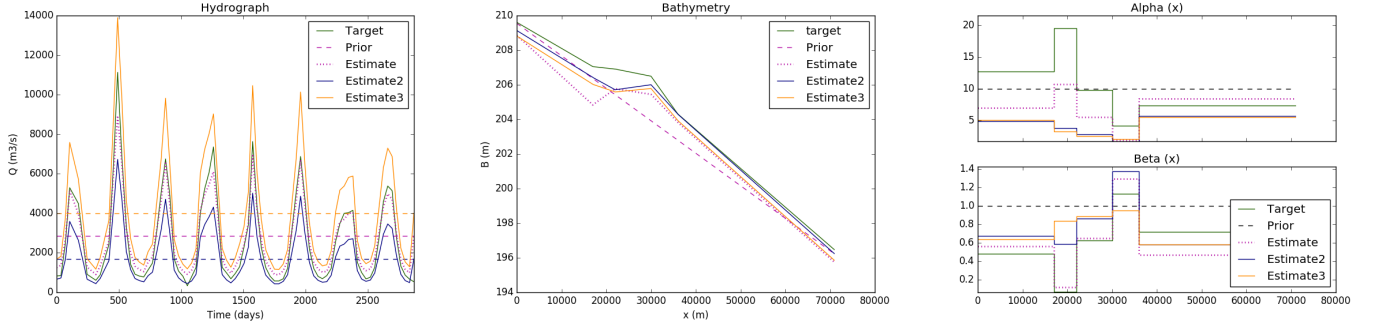


Figure 8: Sensitivity test to the prior discharge  $\overline{Q_{MGB}} \pm 30\%$  ; identification (var change) of  $(Q(t), K(x, h), b(x))$  with ENVISAT observations  $c = (Q_{in,0}, \dots, Q_{in,P}; b_1, \dots, b_R; \alpha_1, \dots, \alpha_S, \beta_1, \dots, \beta_S)^T$  with  $P = 77, R = 6, N = 5$  and with a piecewise linear  $b(x)$  and  $S = R = 5$ . “Estimate” (case Env.b)  $j_{obs} = 0.118$  at iteration 51, “Estimate2” (case Env.b21)  $j_{obs} = 0.125$  at iteration 41, “Estimate3” (case Env.b21)  $j_{obs} = 0.125$  at iteration 25.

355 Next, the sensitivity to the prior bathymetry and friction is tested. The prior bathymetry is inferred with the  
 356 low-complexity system proposed in the hierarchical HiVDI model chain ([1]) for ungauged rivers. It consists in  
 357 estimating an effective prior bathymetry from WS observables using the low Froude model and prior discharge from  
 358 a hydrological model ( $\overline{Q_{MGB}}$  here) and prior friction  $(\alpha^{(0)}, \beta^{(0)})$ . Two prior guesses  $c_{man1}$  and  $c_{man2}$  are considered  
 359 with prior friction under/over-estimations compared to calibrated ones (cf. Fig. 9). As shown on Fig. 9, the  
 360 inference in case Env.b31 (blue) results in an accurate estimation of discharge, very similar to Env.b (purple). It is  
 361 started from a prior guess  $c_{man1}$  that underestimates river bottom elevation and overestimates the spatially averaged  
 362 friction effect compared to calibrated values (cf. Fig. 9, bottom). In that case, fitting WS elevations enables to infer  
 363 an effective river channel (bathymetry and friction) but also to infer a fairly realistic upstream temporal control  
 364 (discharge hydrograph). Using the prior guess  $c_{man2}$  that overestimates both river bottom elevation and spatially  
 365 averaged friction effect results in a comparable fit to the observed WS elevations. However this correct fit stems from  
 366 the compensation between an inferred effective channel of reduced conveyance capacity (comparable friction effects  
 367 but overestimated bed levels) and consequently an inferred hydrograph with underestimated low-flow discharges (in  
 368 yellow).

369

370

### 371 5.2. Spatio-temporal sensitivity of the friction term

372 The considered flow controls  $(Q(t), K(x, h), b(x))$  of the 1D Saint-Venant shallow water equations (Eq. 1)  
 373 have a complex non linear influence on the modeled flow lines and consequently on the fit to the observed ones -  
 374 the latter being evaluated globally in space and time with the current inverse method given the observation cost  
 375 function (Eq. 3). The variation of momentum expressed by the second flow equation is due to a pressure source  
 376 term  $-gA \partial_x Z$  (including the longitudinal variation of fluid-to-fluid pressure, the longitudinal variation of lateral

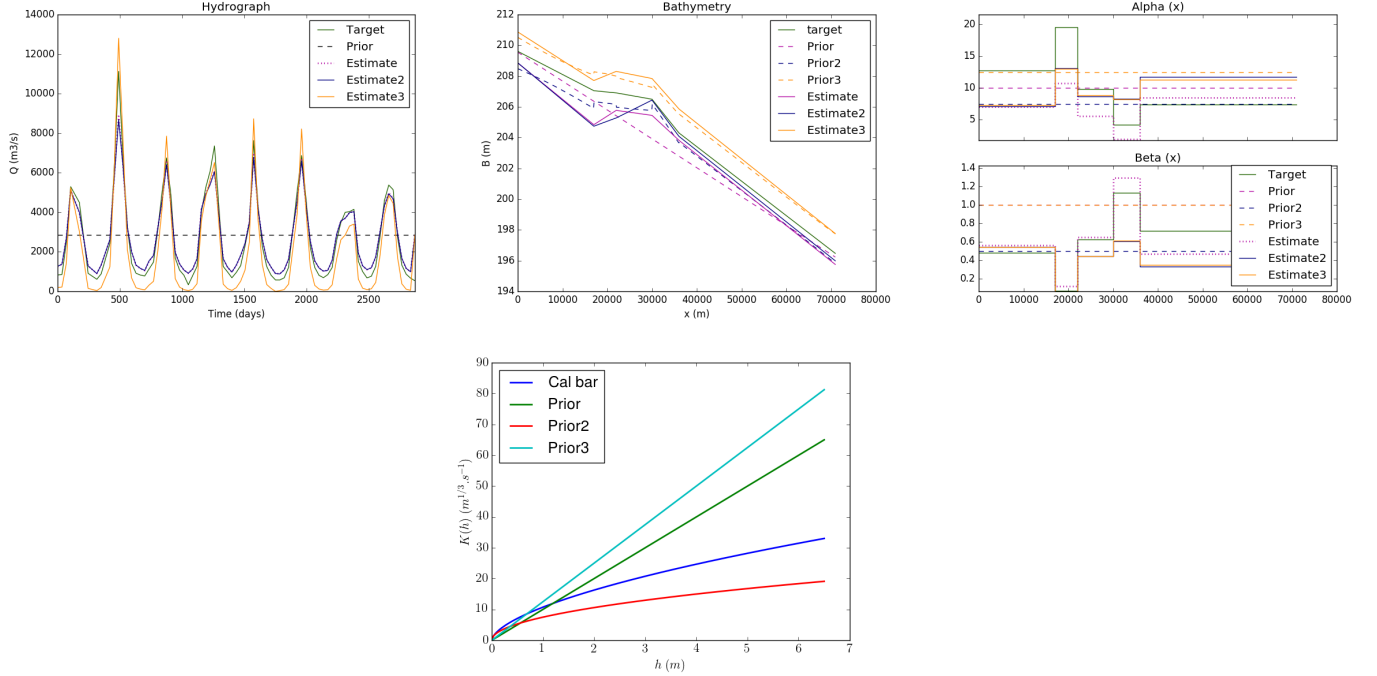


Figure 9: Sensitivity test to the prior friction and bathymetry estimated using the “Manning” method from [1] ( $c_{man1}$  ( $\alpha^{(0)} = 7.5$ ;  $\beta^{(0)} = 0.5$ ) and  $c_{man2}$  ( $\alpha^{(0)} = 12.5$ ;  $\beta^{(0)} = 1$ )); identification (var change) of ( $Q(t), K(x, h), b(x)$ ) with ENVISAT observations  $c = (Q_{in,0}, \dots, Q_{in,P}; b_1, \dots, b_R; \alpha_1, \dots, \alpha_S, \beta_1, \dots, \beta_S)^T$  with  $P = 77, R = 6, N = 5$  and with a piecewise linear  $b(x)$  and  $S = R = 5$ . “Estimate” (case Env.b)  $j_{obs} = 0.118$  at iteration 51, “Estimate2” (case Env.b31)  $j_{obs} = 0.116$  at iteration 46, “Estimate3” (case Env.b32)  $j_{obs} = 0.122$  at iteration 41. (Bottom) prior effective friction laws and spatially averaged calibrated friction law ( $\bar{\alpha}_{cal} = 10.74$  and  $\bar{\beta}_{cal} = 0.6$ , “Cal bar”).

Case	Control	Prior	RMSE <sub>Q<sup>(0)</sup></sub> (m <sup>3</sup> /s)	rRMSE <sub>Q<sup>(0)</sup></sub> (%)	Nash <sub>Q<sup>(0)</sup></sub> (-)	RMSE <sub>b<sup>(0)</sup></sub> (m)	RMSE <sub>α<sup>(0)</sup></sub> (m <sup>1/3-β</sup> /s)	RMSE <sub>β<sup>(0)</sup></sub> (-)
Env.a	Dense $b(x)$	$c_{prior1}$	2254	194	-0.01	1.19	4.93	0.49
Env.b	Piec. $b(x)$	$c_{prior1}$	”	”	”	”	”	”
Env.c	Piec. $b(x), K(h)$	$c_{prior1}$	”	”	”	”	”	”
SWOT.a	Dense $b(x)$	$c_{prior1}$	”	”	”	”	”	”
Env.b21	Piec. $b(x)$	$Q_{prior1}^{(0)} - 30\%$	2433	97	0.18	1.19	4.93	0.49
Env.b22	Piec. $b(x)$	$Q_{prior1}^{(0)} + 30\%$	2626	297	-0.37	”	”	”
Env.b31	Piec. $b(x)$	$c_{man1}$ ( $\alpha^{(0)} = 7.5; \beta^{(0)} = 0.5$ )	2254	194	-0.01	0.77	5.63	0.34
Env.d32	Piec. $b(x)$	$c_{man2}$ ( $\alpha^{(0)} = 12.5; \beta^{(0)} = 1$ )	2254	194	-0.01	1.13	5.43	0.49

Case	Control	Prior	RMSE <sub>Q</sub> (m <sup>3</sup> /s)	rRMSE <sub>Q</sub> (%)	Nash <sub>Q</sub> (-)	RMSE <sub>b</sub> (m)	RMSE <sub>α</sub> (m <sup>1/3-β</sup> /s)	RMSE <sub>β</sub> (-)
Env.a	Dense $b(x)$	$c_{prior1}$	830	57	0.86	1.97	10	0.46
Env.b	Piec. $b(x)$	$c_{prior1}$	520	61	0.95	1.07	4.8	0.37
Env.c	Piec. $b(x), K(h)$	$c_{prior1}$	608	58	0.93	1.05	-	-
SWOT.a	Dense $b(x)$	$c_{prior1}$	391	38	0.97	0.91	5.67	0.2
Env.b2	Piec. $b(x)$	$Q_{prior1}^{(0)} - 30\%$	1229	39	0.7	0.48	7.83	0.28
Env.b3	Piec. $b(x)$	$Q_{prior1}^{(0)} + 30\%$	1473	104	0.57	0.75	5.09	0.22
Env.bm2	Piec. $b(x)$	$c_{man1}$ ( $\alpha^{(0)} = 7.5; \beta^{(0)} = 0.5$ )	550	61	0.94	1.22	4.64	0.32
Env.bm3	Piec. $b(x)$	$c_{man2}$ ( $\alpha^{(0)} = 12.5; \beta^{(0)} = 1$ )	885	78	0.84	1.30	5.50	0.35

Table 2: Scores of the inferences (bottom) performed with various priors (top), ENVISAT (“Env”) or SWOT (“SWOT”) observations.

377 and bottom wall-to-fluid pressure) and a dissipation term  $-gAS_f$ . The discharge and the bathymetry appear in  
 378 the momentum and pressure terms while all the flow controls are embedded in the friction source term  $S_f$ . Note  
 379 that for a locally steady uniform flow  $S_f = -\partial_x Z$  and an infinity of friction and bathymetry values can correspond  
 380 to a single value of discharge (cf. Garambois and Monnier [27], Larnier et al. [1]).

381 We propose a simple calculation in order to make appear the sensitivity of the friction term to a change on the  
 382 controls; let us express the differential of  $S_f$  assuming  $Q > 0$ :

$$\begin{aligned} dS_f &= d\left(\frac{1}{K^2} \frac{Q^2}{A^2 R_h^{4/3}}\right) \\ &= -\frac{2}{K^3} \frac{Q^2}{A^2 R_h^{4/3}} dK - \frac{2}{A^3} \frac{Q^2}{K^2 R_h^{4/3}} dA - \frac{4}{3R_h^{7/3}} \frac{Q^2}{K^2 A^2} dR_h + \frac{1}{K^2} \frac{2Q}{A^2 R_h^{4/3}} dQ \end{aligned} \quad (5)$$

383  
 384 Since  $dR_h = d(A/P) = \frac{1}{P}dA - \frac{A}{P^2}dP = \frac{1}{P}(dA - R_h dP) = \frac{1}{P}(dA_0 - R_h dP_0) + df(h)$  with  $A_0 = W_0 h_0$  and  
 385  $P_0 = W_0 + 2h_0$  respectively the unobserved low-flow area and perimeter under our modeling hypothesis (cf. section  
 386 2.2 and Fig. 1, see also Larnier et al. [1] for details on cross section representation). It follows that  $f(h)$  is a function  
 387 depending on the modeled water depth  $h$  and of the observed cross-section variation  $\delta A$  above low-flow ( $h_0$ ),  $W_0$   
 388 being defined from observables. We get  $dR_h = \frac{1}{P}\left(1 - \frac{2R_h}{W_0}\right)dA_0 + df(h)$  and finally:

$$dS_f = \frac{1}{K^2} \frac{Q}{A^2 R_h^{4/3}} \left(-2\frac{Q}{K}dK - \frac{Q}{A} \left\{2 + \frac{4}{3} \left(1 - \frac{2R_h}{W_0}\right)\right\} dA_0 + 2dQ\right) - d\phi(h) \quad (6)$$

390 with  $\phi(h) = \frac{4}{3R_h^{7/3}} \frac{Q^2}{K^2 A^2} df(h)$  a function depending on the observed geometry of a cross section above low-flow  
 391 and of the simulated flow ( $A, Q$  hence  $h(A)$  given a channel geometry). We rewrite Eq. 6 as  $dS_f = \partial_K S_f dK +$   
 392  $\partial_{A_0} S_f dA_0 + \partial_Q S_f dQ - d\phi(h)$  and under our modeling hypothesis we have  $\partial_K S_f < 0$ ,  $\partial_{A_0} S_f < 0$ ,  $\partial_Q S_f > 0 \forall x, t$ ,  
 393 i.e. opposite effects of local values of friction  $K$ , low flow area  $A_0$  and simulated local discharge  $Q$  values on  $S_f$ .  
 394 Those terms are plotted on Fig. 10 along the Xingu River, on the model grid, from hydraulic variables simulated  
 395 (forward run) with calibrated parameters (cf. Tab. 1). Note that  $d\phi(h)$  is not studied with this simple method.

396 Interestingly,  $|\partial_K S_f|$  is about 100 times greater than  $|\partial_{A_0} S_f|$  or  $|\partial_Q S_f|$  at high-flow and about 10 times greater  
 397 at low-flow. This is consistent with the singular value of friction that is found 1000 times greater than the one of  
 398 reach averaged discharges by Garambois and Monnier [27] through a singular value decomposition of the normal  
 399 equations of reach averaged Manning equations - applied to 70km of the Garonne River downstream of Toulouse  
 400 (France). In other words, the friction term in the present 1D modeling context must be more sensitive to a change  
 401 in friction than unknown low-flow bathymetry or discharge.

402 Remark that for low-flow,  $S_f$  is more sensitive to discharge than unknown cross sectional area ( $|\partial_Q S_f| > |\partial_{A_0} S_f|$ )  
 403 and conversely for high-flow. Moreover the spatial variability of the three sensitivities is more pronounced at low-flow.

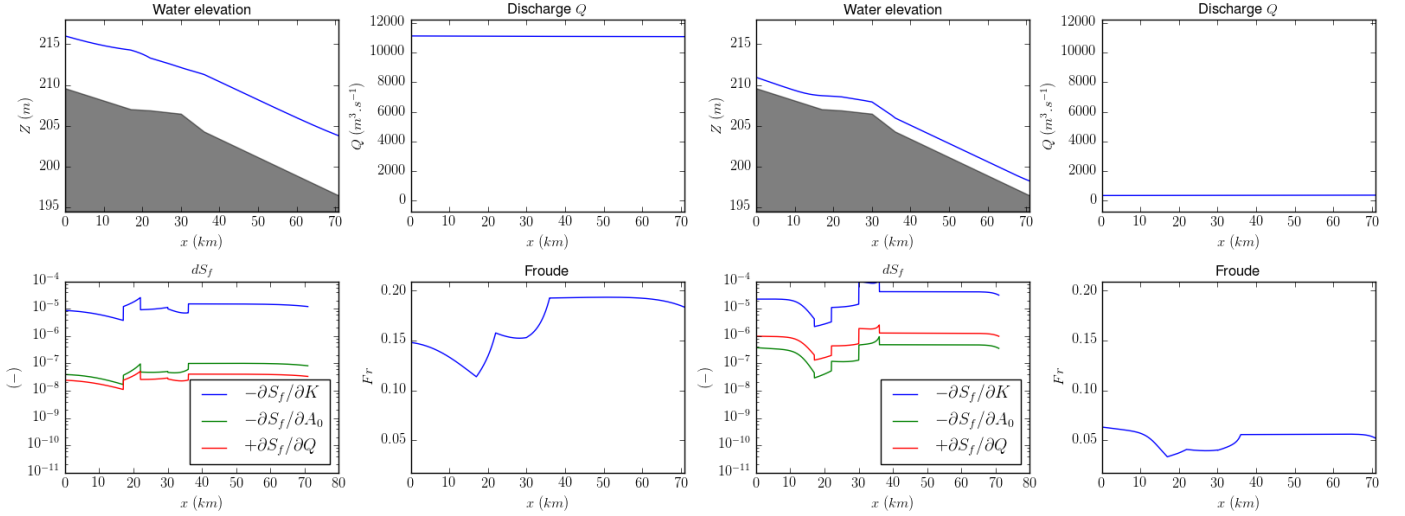


Figure 10: Evaluation of the partial derivatives of the friction source term  $S_f$ ; forward run with the calibrated parameter set (cf. Tab. 1) and true inflow discharge.

404 Abrupt changes are highlighted at locations corresponding to changes in the bottom slope or the channel width.  
 405 The influences of the bottom slope break at  $x = 30\text{km}$  is clearly visible at low-flow and the influence of the width  
 406 contraction at  $x = 17\text{km}$  at high-flow, which is fully consistent with the findings of [3]. Further investigations on  
 407 the sensitivity of the full Saint-Venant equations, and especially the different contributions to the friction slope,  
 408 in space and time could be of interest to better tailor, scale and constrain methods for tackling hydraulic inverse  
 409 problems.

410

## 411 6. Conclusion

412 This paper investigates the challenging inference of the hydraulic triplet (discharge, bathymetry, friction) from  
 413 real or synthetic altimetric WS observations only on an ungauged anabranching river.

414 The HiVDI inverse method presented in [1] is adapted for reproducing an anabranching flow by introducing a  
 415 *spatially distributed* friction law depending on modeled water depth  $h$  and by using multi-satellite data.

416 The friction law coefficients are spatialized by reach to be coherent with the observation grid and with the  
 417 (rather large) meaningful scale of these parameters in the 1D Manning-Strickler equation (see e.g. [61]). This  
 418 effective modeling approach enables a fairly accurate reproduction of the anabranching flows observed during 8  
 419 years by nadir altimetry (ENVISAT) on this  $71\text{km}$  anabranching river.

420 The inference capabilities of hydraulic parameters patterns from real altimetric observations along a single  
 421 ENVISAT track or from the future spatially dense SWOT observations are demonstrated. For the present observed  
 422 anabranching river complexity, the inverse method enables to infer a fairly realistic upstream discharge hydrograph  
 423 along with an effective river channel. The estimated bathymetry and friction patterns somehow result in local

424 and effective stage-discharge relationships. In case of spatially sparse observations, the coherence between the  
425 sparse observation grid and the dense model grid is ensured using a piecewise linear bathymetry representation  
426 along with a friction power law with piecewise constant parameters. This constrain on the VDA process provided  
427 by the above defined effective bathymetry-friction representation by reach is highlighted with spatially sparse  
428 ENVISAT observations. Moreover the additional constrain provided by the forthcoming SWOT observations to  
429 infer a discharge hydrograph and densely distributed spatial controls is assessed on this effective anabranching river  
430 representation; the definition of friction by reaches enabling to consider more dense bathymetry controls.

431 SWOT observations would represent unprecedented measurements of hydrological and hydraulic processes sig-  
432 natures from the local to the hydrographic network scales, including complex flow zones such as anabranching ones.  
433 On-going researches focus on the detection and use of various hydraulic signatures in WS as highlighted here for  
434 bottom slope (resp. channel width) breaks in low (resp. high) flows (see WS curvature analysis and SW model  
435 behavior in [3]), on the estimation of reliable prior guesses on the sought parameters, model scaling and inverse  
436 problems at the scale of larger river network portions including complex flow zones.

#### 437 **Author contributions and acknowledgments**

438 The contributions of the respective authors are as follows. Pierre-André Garambois designed the research  
439 plan and performed the numerical investigations and analysis. Pierre-André Garambois, Pascal Finaud-Guyot,  
440 Kevin Larnier and Amanda Montazem contributed to the hydraulic understanding and sensitivity analysis. Jérôme  
441 Monnier is the principal designer of the inverse computational method and its analysis. Jonas Verley has started  
442 the present study during the beginning of his PhD. This study is warmly dedicated to him.

443 The computational software DassFlow1D and satellite data curation toolbox were adapted from their previous  
444 versions ([1]) by Jonas Verley, Pierre-André Garambois and Kevin Larnier, this last generated the SWOT synthetic  
445 data using the large scale simulator and computational ressources of CNES (“Centre National d’Etudes Spatiales”,  
446 French space agency); Amanda Montazem processed and analyzed the SWOT data. Stéphane Calmant provided  
447 the multisatelite dataset and interesting discussions related to the concept of *hydraulic visibility*.

448 The authors K. Larnier (software engineer at CS corp.) and J. Verley (software engineer during 10 months  
449 next PhD student IMT-INSA-CLS 17-18) have been co-funded by CNES. The four other authors have been partly  
450 supported by CNES TOSCA research project 14-18. The authors are indebted to Adrien Paris and Joecilla Da  
451 Silva for sharing data and for fruitfull discussions.

#### 452 **7. Appendix: the computational inverse method**

453 As already briefly summarized in Section 2.3, the computational inverse method is based on Variational Data  
454 Assimilation (VDA) applied to the Saint-Venant flow model (1). The computational inverse method is those  
455 presented in [36, 1] with an augmented composite control vector  $c$ , see (4):  $c$  contains a spatially distributed friction

456 coefficient enabling to model complex flow zones (while it is an uniform friction law  $K(h)$  in [1]). This definition of  
 457  $K(x, h)$  enables to consider more heterogeneous bathymetry controls.

458 It is important to point out that the imposed downstream boundary condition is an unknown of the inverse  
 459 problem. It is constrained with the observed water elevations and inferred river bottom slope using a locally uniform  
 460 flow hypothesis (i.e. Manning equation, cf. section 2.1).

461 The cost function  $j(c)$  is defined as:

462

$$j(c) = j_{obs}(c) + \gamma j_{reg}(c) \quad (7)$$

463 where  $\gamma > 0$  is a weighting coefficient of the so-called “regularization term”  $j_{reg}(c)$ . The term  $j_{obs}(c)$  measures the  
 464 misfit between observed and modeled WS elevations such that:

465

$$j_{obs}(c) = \frac{1}{2} \|Z(c) - Z_{obs}\|_{\mathcal{O}}^2 \quad (8)$$

466 The norm  $\|\cdot\|_{\mathcal{O}} = \|\mathcal{O}^{1/2}\cdot\|_2$  is defined from an a-priori positive definite covariance matrix  $\mathcal{O}$ . Assuming uncorrelated  
 467 observations  $\mathcal{O} = \text{diag}(\sigma_Z)$  with  $\sigma_Z$  the a-priori observation error on  $Z_{obs}$  -  $\sigma_Z = 15\text{cm}$  in this study.

468 The modeled WS elevations  $Z$  depend on  $c$  through the hydrodynamic model (1) and the inverse problem reads  
 469 as

$$c^* = \text{argmin}_c j(c) \quad (9)$$

470 This optimal control problem is solved using a Quasi-Newton descent algorithm: the L-BFGS algorithm version  
 471 presented in [62]. The cost gradient  $\nabla j(c)$  is computed by solving the adjoint model; the latter is obtained by  
 472 automatic differentiation using Tapenade software [63]. Detailed know-hows on VDA may be found e.g. in the  
 473 online courses [64, 57].

474 To be solved efficiently this optimization problem needs to be “regularized”. Indeed the friction and the  
 475 bathymetry may trigger indiscernible surface signatures therefore leading to an ill-posed inverse problem; we refer  
 476 e.g. to [59] for the theory of regularization of such inverse problems and to [1] for a discussion focused on the present  
 477 inverse flow problem.

478 Following [1], the optimization problem (9) is regularized as follows. First the regularization term  $j_{reg}$  is added  
 479 to the cost function, see (7). We simply set:  $j_{reg}(c) = \frac{1}{2} \|b(x)\|_2^2$ . Therefore this term imposes (as weak constraint)  
 480 the inferred bathymetry profile  $b(x)$  to be an elastic interpolating the values of  $b$  at the control points (i.e. a cubic  
 481 spline).

482 A specificity of the present context is the inconsistency between the large observation grid (altimetry points)  
 483 and the finer model grid. Between the sparse observations points (equivalently the control points), the bathymetry  
 484 profile  $b(x)$  is reconstructed as a piecewise linear function. It is worth to point out that the resulting reconstruction  
 485 is consistent with the physical analysis presented in [20, 60, 3]. (This study analyses the adequation between the

486 SW model (1) behavior and the WS signature).

487 Next and following [65, 66, 1], the following change of control variable is made:

488

$$k = B^{-1/2}(c - c_{prior}) \quad (10)$$

489 where  $c$  is the original control vector,  $c_{prior}$  is a prior value of  $c$  and  $B$  is a covariance matrix. The choice of  $B$  is  
 490 crucial in the VDA formulation; its expression is detailed below. After this change of variable the new optimization  
 491 problem reads:

492

$$\min_k J(k) \text{ with } J(k) = j(c) \quad (11)$$

493

494 It is easy to show that this leads to the following new optimality condition:  $B^{1/2}\nabla j(c) = 0$ ; somehow a  
 495 preconditioned optimality condition. For more details and explanations we refer to [67, 68] and [1] in the present  
 496 inversion context.

497 Assuming uncorrelated controls  $B$  is defined as a block-diagonal matrix:

498

$$B = \begin{pmatrix} B_Q & 0 & 0 & & \\ 0 & B_b & 0 & & \\ 0 & 0 & B_\alpha & & \\ 0 & 0 & 0 & B_\beta & \end{pmatrix} \quad (12)$$

499

500 Still following [1], the matrices  $B_Q$  and  $B_b$  are set as the classical second order auto-regressive correlation  
 501 matrices :

502

$$(B_Q)_{i,j} = (\sigma_Q)^2 \exp\left(-\frac{|t_j - t_i|}{\Delta t_Q}\right) \text{ and } (B_b)_{i,j} = (\sigma_b)^2 \exp\left(-\frac{|x_j - x_i|}{L_b}\right) \quad (13)$$

503

504 The VDA parameters  $\Delta t_Q$  and  $L_b$  represent prior hydraulic scales and act as correlation lengths. Given the fre-  
 505 quency (few days) and spatial resolution of observations (200m long “pixels” for SWOT), the low Froude anabranch-  
 506 ing river flows of interest, adequate values for those parameters are:  $\Delta t_Q = 24$  h and  $L_b = 3km$  km We refer to [36]  
 507 for a thorough analysis of the discharge inference in terms of frequencies and wave lengths and Section 4.1 in the  
 508 present river-observation context. In the present study, the friction parameters applied to deca-kilometric patches  
 509 are assumed to be uncorrelated thus the matrices  $B_\alpha$  and  $B_\beta$  are diagonal:

510

$$(B_\alpha)_{i,i} = (\sigma_\alpha)^2, (B_\beta)_{i,i} = (\sigma_\beta)^2 \quad (14)$$

511

512 The scalar values  $\sigma_{\square}$  may be viewed as variances and constant values are used in this study:  $\sigma_Q = 3500 \text{ m}^3/\text{s}$ ,  
513  $\sigma_{\alpha} = 10 \text{ m}^{1/3} \cdot \text{s}^{-1}$ ,  $\sigma_{\beta} = 0.5$ ,  $\sigma_b = 1 \text{ m}$  .

## 514 8. References

515

- 516 [1] K. Larnier, J. Monnier, P.-A. Garambois, and J. Verley. River discharge and bathymetry estimations from  
517 swot altimetry measurements. -, -:-, 2019.
- 518 [2] Pierre-Andre Garambois, Stephane Calmant, Helene Roux, Adrien Paris, Jerome Monnier, Pascal Finaud-  
519 Guyot, Amanda Samine Montazem, and Joecila Santos-da Silva. Hydraulic visibility: Using satellite altimetry  
520 to parameterize a hydraulic model of an ungauged reach of a braided river. *Hydrological Processes*, 31(4):  
521 756–767, 2017. ISSN 1099-1085. doi: 10.1002/hyp.11033. URL <http://dx.doi.org/10.1002/hyp.11033>.  
522 hyp.11033.
- 523 [3] A.-S. Montazem, P.-A. Garambois, S. Calmant, P. Finaud-Guyot, J. Monnier, D. Medeiros Moreira, J. T.  
524 Minear, and S. Biancamaria. Wavelet-based river segmentation using hydraulic control-preserving water surface  
525 elevation profile properties. *Geophysical Research Letters*, 46(12):6534–6543, 2019. doi: 10.1029/2019GL082986.  
526 URL <https://agupubs.onlinelibrary.wiley.com/doi/abs/10.1029/2019GL082986>.
- [4] World Meteorological Organization et al. The global observing system for climate: Implementation needs,  
2016. URL [library.wmo.int/doc\\_num.php?explnum\\_id=3417](http://library.wmo.int/doc_num.php?explnum_id=3417).
- 527 [5] B.M. Fekete and C.J. Vorosmarty. The current status of global river discharge monitoring and potential new  
528 technologies complementing traditional discharge measurements. *IAHS - PUB*, 2002.
- 529 [6] Charles J. Vorosmarty, Cort J. Willmott, Bhaskar J. Choudhury, Annette L. Schloss, Timothy K. Stearns,  
530 Scott M. Robeson, and Timothy J. Dorman. Analyzing the discharge regime of a large tropical river through  
531 remote sensing, ground-based climatic data, and modeling. *Water Resour. Res.*, 32:3137–3150, 1996. URL  
532 <http://dx.doi.org/10.1029/96WR01333>. 10.
- 533 [7] Douglas E. Alsdorf and Dennis P. Lettenmaier. Tracking fresh water from space. *Science*, 301(5639):1491–1494,  
534 2003. doi: 10.1126/science.1089802. URL <http://www.sciencemag.org/content/301/5639/1491.short>.
- 535 [8] Stephane Calmant, Frederique Seyler, and Jean-Francois Cretaux. Monitoring continental surface waters by  
536 satellite altimetry. *Surveys in Geophysics*, 29(4-5):247–269, 2008. ISSN 0169-3298. doi: 10.1007/s10712-008-  
537 9051-1. URL <http://dx.doi.org/10.1007/s10712-008-9051-1>.

- 538 [9] G. J.-P. Schumann and A. Domeneghetti. Exploiting the proliferation of current and future satellite  
539 observations of rivers. *Hydrological Processes*, 30(16):2891–2896, 2016. doi: 10.1002/hyp.10825. URL  
540 <https://onlinelibrary.wiley.com/doi/abs/10.1002/hyp.10825>.
- 541 [10] Douglas E. Alsdorf, Ernesto Rodríguez, and Dennis P. Lettenmaier. Measuring surface wa-  
542 ter from space. *Reviews of Geophysics*, 45(2), 2007. doi: 10.1029/2006RG000197. URL  
543 <https://agupubs.onlinelibrary.wiley.com/doi/abs/10.1029/2006RG000197>.
- 544 [11] M. Durand, L. Fu, D. P. Lettenmaier, D. E. Alsdorf, E. Rodriguez, and D. Esteban-Fernandez. The surface  
545 water and ocean topography mission: Observing terrestrial surface water and oceanic submesoscale eddies.  
546 *Proceedings of the IEEE*, 98(5):766–779, May 2010. doi: 10.1109/JPROC.2010.2043031.
- 547 [12] E. Rodriguez. SWOT Science requirements document. JPL document, JPL, 2012.
- 548 [13] Sylvain Biancamaria, Dennis P. Lettenmaier, and Tamlin M. Pavelsky. The swot mission and its capabilities  
549 for land hydrology. *Surveys in Geophysics*, 37(2):307–337, Mar 2016. ISSN 1573-0956. doi: 10.1007/s10712-  
550 015-9346-y. URL <http://dx.doi.org/10.1007/s10712-015-9346-y>.
- 551 [14] E. Rodriguez, Esteban-Fernandez D., E. Peral, C. W. Chen, J.-W. d. Blesser, and B. Williams. Wide-swath  
552 altimetry: A review. in d. stammer a. cazenave (eds.). *Satellite Altimetry over Oceans and Land Surfaces*  
553 (*Chapter 2*), page CRC press, 2018.
- 554 [15] Frederic Frappart, Stephane Calmant, Mathilde Cauhope, Frederique Seyler, and Anny Cazenave. Prelim-  
555 inary results of envisat ra-2-derived water levels validation over the amazon basin. *Remote Sensing of En-*  
556 *vironment*, 100(2):252 – 264, 2006. ISSN 0034-4257. doi: <https://doi.org/10.1016/j.rse.2005.10.027>. URL  
557 <http://www.sciencedirect.com/science/article/pii/S0034425705003585>.
- 558 [16] Charon M. Birkett. Contribution of the topeX nasa radar altimeter to the global monitoring of large  
559 rivers and wetlands. *Water Resources Research*, 34(5):1223–1239, 1998. doi: 10.1029/98WR00124. URL  
560 <https://agupubs.onlinelibrary.wiley.com/doi/abs/10.1029/98WR00124>.
- 561 [17] Joecila Santos Da Silva, Frederique Seyler, Stephane Calmant, Otto Correa Rotunno Filho, Emmanuel Roux,  
562 Afonso Augusto Magalhaes Arango, and Jean Loup Guyot. Water level dynamics of amazon wetlands at the  
563 watershed scale by satellite altimetry. *International Journal of Remote Sensing*, 33(11):3323–3353, 2012. doi:  
564 10.1080/01431161.2010.531914. URL <http://dx.doi.org/10.1080/01431161.2010.531914>.
- 565 [18] S. Calmant, J.-F. Cretaux, and F. Remy. 4 - principles of radar satellite altimetry for application on inland  
566 waters. In Nicolas Baghdadi and Mehrez Zribi, editors, *Microwave Remote Sensing of Land Surface*, pages  
567 175 – 218. Elsevier, 2016. ISBN 978-1-78548-159-8. doi: <https://doi.org/10.1016/B978-1-78548-159-8.50004-9>.  
568 URL <https://www.sciencedirect.com/science/article/pii/B9781785481598500049>.

- 569 [19] George H. Allen and Tamlin M. Pavelsky. Global extent of rivers and  
570 streams. *Science*, 2018. ISSN 0036-8075. doi: 10.1126/science.aat0636. URL  
571 <http://science.sciencemag.org/content/early/2018/06/27/science.aat0636>.
- 572 [20] A. S. Montazem, P.-A. Garambois, S. Calmant, D. Medeiros Moreira, J. Monnier, and S. Biancamaria. Physical  
573 basis for river segmentation. In *AGU fall meeting*, 2017.
- 574 [21] G. C. Nanson and A. D. Knighton. Anabranching rivers: Their cause, character and classification. *Earth*  
575 *Surface Processes and Landforms*, 21(3):217–239, 1996.
- 576 [22] Konstantinos M. Andreadis, Elizabeth A. Clark, Dennis P. Lettenmaier, and Douglas E. Alsdorf. Prospects  
577 for river discharge and depth estimation through assimilation of swath-altimetry into a raster-based hy-  
578 drodynamics model. *Geophysical Research Letters*, 34(10), 2007. doi: 10.1029/2007GL029721. URL  
579 <https://agupubs.onlinelibrary.wiley.com/doi/abs/10.1029/2007GL029721>.
- 580 [23] S. Biancamaria, M. Durand, K.M. Andreadis, P.D. Bates, A. Boone, N.M. Mognard, E. Ro-  
581 driguez, D.E. Alsdorf, D.P. Lettenmaier, and E.A. Clark. Assimilation of virtual wide  
582 swath altimetry to improve arctic river modeling. *Remote Sensing of Environment*, 115(2):  
583 373 – 381, 2011. ISSN 0034-4257. doi: <https://doi.org/10.1016/j.rse.2010.09.008>. URL  
584 <http://www.sciencedirect.com/science/article/pii/S0034425710002816>.
- 585 [24] Michael Durand, Konstantinos M. Andreadis, Douglas E. Alsdorf, Dennis P. Lettenmaier, Delwyn Moller,  
586 and Matthew Wilson. Estimation of bathymetric depth and slope from data assimilation of swath altimetry  
587 into a hydrodynamic model. *Geophysical Research Letters*, 35(20), 2008. doi: 10.1029/2008GL034150. URL  
588 <https://agupubs.onlinelibrary.wiley.com/doi/abs/10.1029/2008GL034150>.
- 589 [25] Y. Yoon, M. Durand, C.J. Merry, E.A. Clark, K.M. Andreadis, and Alsdorf D.E. Estimating river  
590 bathymetry from data assimilation of synthetic swot measurements. *Journal of Hydrology*, 464 - 465  
591 (0):363 – 375, 2012. ISSN 0022-1694. doi: <http://dx.doi.org/10.1016/j.jhydrol.2012.07.028>. URL  
592 <http://www.sciencedirect.com/science/article/pii/S0022169412006294>.
- 593 [26] Michael Durand, Jeffrey Neal, Ernesto Rodríguez, Konstantinos M Andreadis, Laurence C Smith, and Yeosang  
594 Yoon. Estimating reach-averaged discharge for the river severn from measurements of river water surface  
595 elevation and slope. *Journal of Hydrology*, 511:92–104, 2014.
- 596 [27] P-A. Garambois and J. Monnier. Inference of effective river properties from remotely sensed observations of  
597 water surface. *Advances in Water Resources*, 79:103–120, 2015.
- 598 [28] Colin J. Gleason and Laurence C. Smith. Toward global mapping of river discharge using satellite images and

- at-many-stations hydraulic geometry. *Proceedings of the National Academy of Sciences*, 111(13):4788–4791, 2014. ISSN 0027-8424. doi: 10.1073/pnas.1317606111. URL <http://www.pnas.org/content/111/13/4788>.
- [29] M. Durand, C.J. Gleason, P-A. Garambois, D. Bjerklie, L.C. Smith, H. Roux, E. Rodriguez, P.D. Bates, T.M. Pavelsky, J Monnier, et al. An intercomparison of remote sensing river discharge estimation algorithms from measurements of river height, width, and slope. *Water Resources Research*, 2016.
- [30] David M. Bjerklie, Charon M. Birkett, John W. Jones, Claudia Carabajal, Jennifer A. Rover, John W. Fulton, and Pierre-Andre Garambois. Satellite remote sensing estimation of river discharge: Application to the yukon river alaska. *Journal of Hydrology*, 561:1000 – 1018, 2018. ISSN 0022-1694. doi: <https://doi.org/10.1016/j.jhydrol.2018.04.005>. URL <http://www.sciencedirect.com/science/article/pii/S0022169418302464>.
- [31] H. Roux and D. Dartus. Use of parameter optimization to estimate a flood wave: Potential applications to remote sensing of rivers. *J. of Hydrology*, 328:258–266, 2006.
- [32] M. Honnorat, X. Lai, F-X. le Dimet, and J. Monnier. Variational data assimilation for 2D fluvial hydraulics simulation. *CMWR XVI-Computational Methods for Water Ressources. Copenhagen, june 2006.*, 2006.
- [33] R. Hostache, X. Lai, J Monnier, and C. Puech. Assimilation of spatially distributed water levels into a shallow-water flood model. Part II: Use of a remote sensing image of Mosel River. *Journal of Hydrology*, 390:257–268, 2010. URL <http://www.sciencedirect.com/science/article/pii/S0022169410004166>. 3-4.
- [34] X. Lai and J. Monnier. Assimilation of spatially distributed water levels into a shallow-water flood model. Part I: mathematical method and test case. *Journal of Hydrology*, 377:1–11, 2009. URL <http://www.sciencedirect.com/science/article/pii/S0022169409004508>. 1-2.
- [35] DG Cacuci, IM, Navon, and M, Ionescu-Bugor. *Computational Methods for Data Evaluation and Assimilation*. Taylor and Francis CRC Press: Boca Raton, 2013.
- [36] Pierre Brisset, Jérôme Monnier, Pierre-André Garambois, and Hélène Roux. On the assimilation of altimetric data in 1d saint-venant river flow models. *Advances in water resources*, 119:41–59, 2018.
- [37] H. Oubanas, Igor Gejadze, Pierre-Olivier Malaterre, and F. Mercier. River discharge estimation from synthetic swot-type observations using variational data assimilation and the full saint-venant hydraulic model. *Journal of Hydrology*, pages Accepted, to appear, 2018.
- [38] Igor Gejadze and Pierre-Olivier Malaterre. Discharge estimation under uncertainty using variational methods with application to the full saint-venant hydraulic network model. *International Journal for Numerical Methods in Fluids*, 83(5):405–430, 2017. ISSN 1097-0363. doi: 10.1002/flid.4273. URL <http://dx.doi.org/10.1002/flid.4273>. flid.4273.

- 630 [39] Y. Yoon, P-A. Garambois, R. Paiva, M. Durand, H. Roux, and E. Beighley. Improved error estimates of a  
631 discharge algorithm for remotely sensed river measurements: Test cases on Sacramento and Garonne Rivers.  
632 *Water Resources Research*, 52(1):278–294, 2016.
- 633 [40] S. Tuozzolo, G. Lind, B. Overstreet, J. Mangano, M. Fonstad, M. Hagemann, R. P. M. Frasson, K. Larnier,  
634 P-A. Garambois, J. Monnier, and M. Durand. Estimating river discharge with swath altimetry: A proof of  
635 concept using airswot observations. *Geophysical Research Letters*, 0(ja), 2019. doi: 10.1029/2018GL080771.  
636 URL <https://agupubs.onlinelibrary.wiley.com/doi/abs/10.1029/2018GL080771>.
- 637 [41] A. F. Gessese, M. Sellier, E. Van Houten, and G. Smart. Reconstruction of river bed topography from free  
638 surface data using a direct numerical approach in one-dimensional shallow water flow. *Inverse Problems*, 27  
639 (2):025001, 2011. URL <http://stacks.iop.org/0266-5611/27/i=2/a=025001>.
- 640 [42] R. Schneider, P. N. Godiksen, H. Villadsen, H. Madsen, and P. Bauer-Gottwein. Application of cryosat-2  
641 altimetry data for river analysis and modelling. *Hydrology and Earth System Sciences*, 21(2):751–764, 2017.  
642 doi: 10.5194/hess-21-751-2017. URL <https://www.hydro1-earth-syst-sci.net/21/751/2017/>.
- 643 [43] Jochen E. Schubert, Wade W. Monsen, and Brett F. Sanders. Metric-resolution 2d river mod-  
644 eling at the macroscale: Computational methods and applications in a braided river. *Frontiers in Earth Science*,  
645 3:74, 2015. ISSN 2296-6463. doi: 10.3389/feart.2015.00074. URL  
646 <https://www.frontiersin.org/article/10.3389/feart.2015.00074>.
- 647 [44] V.T. Chow. Handbook of applied hydrology. *McGraw-Hill Book Co., New-York, 1467 pages*, 1964.
- 648 [45] V. Guinot. *Wave Propagation in Fluids: Models and Numerical Techniques*, volume 16. 1993.
- 649 [46] David M. Bjerklie, S. Lawrence Dingman, and Carl H. Bolster. Comparison of constitu-  
650 tive flow resistance equations based on the manning and chezy equations applied to natu-  
651 ral rivers. *Water Resources Research*, 41(11), 2005. doi: 10.1029/2004WR003776. URL  
652 <https://agupubs.onlinelibrary.wiley.com/doi/abs/10.1029/2004WR003776>.
- 653 [47] Rob Ferguson. Flow resistance equations for gravel- and boulder-bed streams.  
654 *Water Resources Research*, 43(5), 2007. doi: 10.1029/2006WR005422. URL  
655 <https://agupubs.onlinelibrary.wiley.com/doi/abs/10.1029/2006WR005422>.
- 656 [48] V.T. Chow. *Open-channel Hydraulics*. Mc Graw-Hill, New-York, USA, 1959.
- 657 [49] P-A. Garambois and J. Monnier. Inference of effective river properties from remotely sensed observations of  
658 water surface. *Advances in Water Resources*, 79:103–120, 2015.
- 659 [50] J. A. Cunge, M. Holly, F., and A. Verwey. *Practical Aspects of Computational River Hydraulics*. Pitam  
660 Publishing, 1980.

- 661 [51] DassFlow. Data assimilation for free surface flows. Technical report, Mathematics Institute of  
662 Toulouse-INSA group-CS corp.-CNES-CNRS. <http://www.math.univ-toulouse.fr/DassFlow>, 2019. URL  
663 <http://www.math.univ-toulouse.fr/DassFlow>.
- 664 [52] A. Paris, R. Dias de Paiva, J. Santos da Silva, D. Medeiros Moreira, S. Calmant, P.-A. Garambois, W. Col-  
665 lischonn, M.-P. Bonnet, and F. Seyler. Stage-discharge rating curves based on satellite altimetry and modeled  
666 discharge in the amazon basin. *Water Resources Research*, 52(5):3787–3814, 2016. doi: 10.1002/2014WR016618.  
667 URL <https://agupubs.onlinelibrary.wiley.com/doi/abs/10.1002/2014WR016618>.
- 668 [53] Walter Collischonn, Daniel Allasia, B. Da Silva, and C. E. M. Tucci. The mgb-iph model for large-scale  
669 rainfall-runoff modelling. *Hydrological Sciences Journal*, 52(5):878–895, 2007. doi: 10.1623/hysj.52.5.878.
- 670 [54] R. Paiva, D. Costa Buarque, W. Collischonn, M.-P. Bonnet, F. Frappart, S. Calmant, and  
671 C. Bulhoes Mendes. Large-scale hydrologic and hydrodynamic modeling of the amazon river  
672 basin. *Water Resources Research*, 49(3):1226–1243, 2013. doi: 10.1002/wrcr.20067. URL  
673 <https://agupubs.onlinelibrary.wiley.com/doi/abs/10.1002/wrcr.20067>.
- 674 [55] P. R. M. Pontes, F. M. Fan, A. S. Fleischmann, R. C. D. Paiva, D. C. Buarque, V. A. Siqueira, Pe-  
675 dro F. J., M. V. Sorribas, and W. Collischonn. Mgb-iph model for hydrological and hydraulic simu-  
676 lation of large floodplain river systems coupled with open source gis. *Environmental Modelling Soft-*  
677 *ware*, 94:1 – 20, 2017. ISSN 1364-8152. doi: <https://doi.org/10.1016/j.envsoft.2017.03.029>. URL  
678 <http://www.sciencedirect.com/science/article/pii/S136481521630189X>.
- 679 [56] J. Monnier, F. Couderc, D. Dartus, K. Larnier, R. Madec, and J-P. Vila. Inverse algorithms for 2D shallow  
680 water equations in presence of wet dry fronts. application to flood plain dynamics. *Advances in Water Resources*,  
681 97:11–24, 2016.
- 682 [57] J. Monnier. *Variational data assimilation: from optimal control to large scale data assimilation*. Open Online  
683 Course, INSA Toulouse, 2014.
- 684 [58] Renato Prata de Moraes Frasson, Rui Wei, Michael Durand, J. Toby Minear, Alessio Domeneghetti, Guy  
685 Schumann, Brent A. Williams, Ernesto Rodriguez, Christophe Picamilh, Christine Lion, Tamlin Pavelsky,  
686 and Pierre-Andre Garambois. Automated river reach definition strategies: Applications for the surface water  
687 and ocean topography mission. *Water Resources Research*, 53(10):8164–8186, 2017. ISSN 1944-7973. doi:  
688 10.1002/2017WR020887. URL <http://dx.doi.org/10.1002/2017WR020887>.
- 689 [59] Barbara Kaltenbacher, Andreas Neubauer, and Otmar Scherzer. *Iterative regularization methods for nonlinear*  
690 *ill-posed problems*, volume 6. Walter de Gruyter, 2008.

- 691 [60] Amanda Montazem. *Représentation et segmentation hydraulique effective de rivières pour le calcul de débit par*  
692 *altimétrie SWOT À l'échelle globale*. These de doctorat, Université de Toulouse III Paul Sabatier, Toulouse,  
693 France, 2018.
- 694 [61] Vincent Guinot and Bernard Cappelaere. Sensitivity equations for the one-dimensional shallow water equations:  
695 Practical application to model calibration. *Journal of Hydrologic Engineering*, 14(8):858–861, 2009. doi:  
696 10.1061/(ASCE)HE.1943-5584.0000061.
- 697 [62] J. C. Gilbert and C. Lemarechal. Some numerical experiments with variable-storage quasi-newton algorithms.  
698 *Mathematical programming*, 45(1-3):407–435, 1989.
- 699 [63] L. Hascoët and V. Pascual. The Tapenade Automatic Differentiation tool: Principles,  
700 Model, and Specification. *ACM Transactions On Mathematical Software*, 39(3), 2013. URL  
701 <http://dx.doi.org/10.1145/2450153.2450158>.
- 702 [64] F. Bouttier and P. Courtier. Data assimilation concepts and methods march 1999. *Meteorological training course*  
703 *lecture series*. ECMWF, page 59, 2002.
- 704 [65] A.C. Lorenc, S.P. Ballard, R.S. Bell, N.B. Ingleby, P.L.F. Andrews, D.M. Barker, J.R. Bray, A.M. Clayton,  
705 T. Dalby, D. Li, et al. The met. office global three-dimensional variational data assimilation scheme. *Quarterly*  
706 *Journal of the Royal Meteorological Society*, 126(570):2991–3012, 2000.
- 707 [66] A. Weaver and P. Courtier. Correlation modelling on the sphere using a generalized diffusion equation. *Quar-*  
708 *terly Journal of the Royal Meteorological Society*, 127(575):1815–1846, 2001.
- 709 [67] Stephen A Haben, Amos S Lawless, and Nancy K Nichols. Conditioning and preconditioning of the variational  
710 data assimilation problem. *Computers & Fluids*, 46(1):252–256, 2011.
- 711 [68] Stephen A Haben, Amos S Lawless, and Nancy K Nichols. Conditioning of incremental variational data  
712 assimilation, with application to the met office system. *Tellus A*, 63(4):782–792, 2011.